

Studies of PurE from *Bacillus anthracis*: Its Solution Properties and Inhibitors

BY

Anna Jones

B.S., Calvin College, Grand Rapids, 2011

THESIS

Submitted as partial fulfillment of the requirements
for the degree of Doctor of Philosophy in Chemistry
in the Graduate College of the
University of Illinois at Chicago, 2018

Chicago, Illinois

Defense Committee:

Leslie W.-M. Fung, Chair and Advisor, Chemistry

Duncan Wardrop, Chemistry

Jung-Hyun Min, Chemistry

Scott Shippy, Chemistry

Vadim Gaponenko, UIC Department of Biochemistry and Molecular Genetics

ACKNOWLEDGMENT

I thank the University of Illinois at Chicago Chemistry Department for teaching and to Dr. Leslie W. M.- Fung for her research grant (HDTRA 1-11-C0011) in providing research assistantship, in addition to tuition waiver for five years.

I would like to show my gratitude and appreciation to my graduate advisor, Leslie W.-M. Fung for her help in completing this degree. Her help in skills development such as data analysis, presentation, quantitative reasoning skills have been invaluable for me to come this far. I would also like to thank my former lab mate, Dr. Nina M. Wolf for her collaboration for a major part of the project in this dissertation. I extend this thanks for other former and current lab mates, including Dr. Mike Tuntland, Pauline Kabre, Robel Demissie and Truc Phan for their time in contribution of their thoughts involving my project.

AJ

CONTRIBUTION OF AUTHORS

Dr. Nina M. Wolf prepared majority of the protein used in the High Throughput Screening and initiated the design of thermal shift assay carried out in chapter 2 of this dissertation.

Robel Demissie assisted in carrying out the synthesis of a substrate used by the enzyme studied in this dissertation.

TABLE OF CONTENTS

<u>CHAPTER</u>	<u>PAGE</u>
1. INTRODUCTION	
1.1 <u>Antibacterial Resistance</u>	1
1.1.1 <u>Resistance in Bacteria</u>	1
1.1.2 <u>Mechanism of Resistance</u>	1
1.2 <u>Bacillus anthracis</u>	2
1.2.1 <u>de novo Purine Biosynthetic Pathway</u>	2
1.2.2 <u>Enzymes of Prokaryotic Purine Pathway</u>	4
1.2.3 <u>N⁵-Carboxyaminoimidazole Ribonucleotide Mutase</u>	4
1.2.4 <u>Structure-Based Lead Design</u>	5
1.3 <u>Biophysical and Biochemical Methods</u>	5
1.3.1 <u>Preparation of Recombinant Protein</u>	5
1.3.2 <u>Circular Dichroism</u>	6
1.3.2.1 <u>Far UV Region</u>	6
1.3.2.2 <u>Near UV Region</u>	6
1.3.3 <u>Denaturation</u>	8
1.3.3.1 <u>Thermal Denaturation</u>	8
1.3.3.2 <u>Chemical Denaturation</u>	8
1.3.4 <u>Size Exclusion Chromatography - Hydrodynamic Size</u>	9
1.3.5 <u>Assay</u>	9
1.3.5.1 <u>Thermal Shift Assay - Fluorescence</u>	9

1.3.5.2	<u>Assay for PurE Activity and Inhibition - UV Spectroscopy.</u>	10
1.3.6	<u>Tryptophan Fluorescence.</u>	10
1.3.7	<u>High Throughput Screening.</u>	12
2.	A HIGH THROUGHPUT SCREENING FOR INHIBITORS OF PURE FROM <i>BACILLUS ANTHRACIS</i>	
2.1	<u>Introduction.</u>	13
2.2	<u>Experimental Procedures.</u>	14
2.2.1	<u>Sample Preparation</u>	14
2.2.2	<u>Thermal Unfolding Assay with Positive Control.</u>	15
2.2.3	<u>High Throughput Screening by RT-PCR.</u>	16
2.2.4	<u>Hit Selection and Assay Evaluation.</u>	17
2.2.5	<u>In Silico Screening.</u>	17
2.2.6	<u>Enzyme Activity and Inhibition Assay</u>	18
2.2.7	<u>Minimum Inhibitory Concentration.</u>	19
2.3	<u>Results.</u>	19
2.3.1	<u>Dependence of ΔT_m on Ionic Strength.</u>	19
2.3.2	<u>Hit selection and Z'-Factor for Assay Reliability.</u>	22
2.3.3	<u>Inhibition Activity</u>	22
2.3.4	<u>Minimum Inhibitory Concentration.</u>	25
2.3.5	<u>Identification of a Core Structure.</u>	25
2.4	<u>Discussion.</u>	29

2.5 <u>Conclusion</u>	31
-----------------------------	----

3. SOLUTION PROPERTIES OF *BAPURE* AND BIOCHEMICAL AND BIOPHYSICAL CHARACTERIZATION

3.1 <u>Introduction</u>	32
3.2 <u>Experimental Procedures</u>	33
3.2.1 <u>Protein Preparation</u>	33
3.2.2 <u>Size Exclusion Chromatography</u>	33
3.2.3 <u>Enzymatic Activity and Ionic Strength</u>	34
3.2.3.1 <u>CAIR Synthesis</u>	34
3.2.3.2 <u>Samples in Buffers with Different Ionic Strength</u>	35
3.2.4 <u>Circular Dichroism</u>	36
3.2.4.1 <u>Secondary Structure</u>	36
3.2.4.2 <u>Tertiary Structure</u>	36
3.2.5 <u>Fluorescence</u>	36
3.2.5.1 <u>Tryptophan Quenching with Acrylamide</u>	37
3.3 <u>Results</u>	37
3.3.1 <u>Enzymatic Activity Dependence on Ionic Strength</u>	37
3.3.1.1 <u>Buffer conductivity</u>	37
3.3.1.2 <u>CAIR</u>	38
3.3.1.3 <u>Enzymatic Activity Dependence on Ionic Strength</u>	38
3.3.2 <u>Secondary and Tertiary Structural Elements</u>	39

3.3.3	<u>Tryptophan Accessibility.</u>	41
3.4	<u>Discussion.</u>	42
3.5	<u>Conclusion.</u>	43
4.	CHEMICAL UNFOLDING OF <i>BaPurE</i>	
4.1	<u>Introduction.</u>	46
4.2	<u>Experimental Procedures.</u>	47
4.2.1	<u>Protein Preparation.</u>	47
4.2.2	<u>Chemical Unfolding of <i>BaPurE</i> by Circular Dichroism Method.</u>	47
4.3	<u>Results.</u>	49
4.3.1	<u>Chemical Unfolding of <i>BaPurE</i> in Guanidium Chloride.</u>	49
4.3.1.1	<u>Effect of different ionic strength buffer on unfolding.</u>	49
4.3.2	<u>Chemical Unfolding of <i>BaPurE</i> in Urea.</u>	52
4.3.2.1	<u>Effect of different ionic strength buffer on unfolding.</u>	52
4.4	<u>Discussion.</u>	56
4.5	<u>Conclusion.</u>	57
	REFERENCES.	58
	CURRICULUM VITAE.	83
	APPENDIX A.	85

APPENDIX B.	94
APPENDIX C.	95

LIST OF TABLES

<u>TABLE</u>	<u>PAGE</u>
2.1 Inhibition of <i>Ba</i> PurE by hit compounds from HTS.....	24
2.2 Summary of thermal shift hits from HTS.	26
2.3 Structure of inhibitor compounds.	27
3.1 Buffer abbreviation and conductivity.....	38
4.1 Summary of chemical denaturation by Gdn-HCl and urea.	55

LIST OF FIGURES

<u>FIGURE</u>	<u>PAGE</u>
1.1 The <i>de novo</i> purine biosynthetic pathway.	3
2.1 Thermal unfolding profile of <i>BaPurE</i>	20
2.2 Thermal unfolding profile of <i>BaPurE</i> in 25TRIS8-0 or 50TRIS8-0 buffer.....	21
2.3 Activity of 10 nM <i>BaPurE</i> in 25TRIS8-0.	23
2.4 Summary of HTS of <i>BaPurE</i>	28
3.1 Specific activity of <i>BaPurE</i> in different ionic strength.	39
3.2 Secondary structure of <i>BaPurE</i>	40
3.3 Near-UV CD spectrum of <i>BaPurE</i>	41
4.1 Equilibrium denaturation curve of <i>BaPurE</i>	49
4.2 Fraction unfolded versus [Gdn-HCl] and ΔG_D of <i>BaPurE</i> versus [Gdn-HCl].....	51
4.3 Fraction unfolded versus [urea] and ΔG_D of <i>BaPurE</i> versus [urea].....	53

LIST OF ABBREVIATIONS

AICAR	5-Amino-1-(β -D-ribofuranosyl)-4-carboxamide-5'-phosphate
AIR	5-Aminoimidazole ribonucleotide
<i>BaPurE</i>	N ⁵ -CAIR mutase from <i>Bacillus anthracis</i>
CAIR	4-Carboxy-5-aminoimidazole ribonucleotide
CD	Circular Dichroism
DMSO	Dimethylsulfoxide
<i>EcPurE</i>	N ⁵ -CAIR mutase from <i>Escherichia coli</i>
Gdn-HCl	Guanidine hydrochloride
GSH	Glutathione
GST	Glutathione S-transferase
His	Histidine
HTS	High throughput screening
IMP	Inosine monophosphate
IPTG	Isopropyl β -D-1-thiogalactopyranoside
K _{av}	Partition coefficient
KI	Potassium iodide
K _{sv}	Stern-Volmer quenching constant
λ_{max}	Maximum emission wavelength
LB	Luria broth
MIC	Minimum inhibitory concentration
MRE	Mean residue ellipticity

MRSA	Methicillin-resistant <i>Staphylococcus aureus</i>
MSSA	Methicillin-susceptible <i>Staphylococcus aureus</i>
MW _H	Hydrodynamic molar mass
N ⁵ -CAIR	N ⁵ -carboxyaminoimidazole ribonucleotide
NAIR	Nitroaminoimidazole ribonucleotide
Ni-NTA	Nitrilotriacetic acid
PBS	Phosphate (5 mM) buffered saline pH 7.4 with 150 mM NaCl
PCR	Polymerase chain reaction
PDB	Protein data bank
PRPP	5'-phosphoribosyl pyrophosphate
Pur6	Eukaryotic organism's carboxyaminoimidazole ribonucleotide synthase/succinoaminoimidazolecarboxamide ribonucleotide synthetase
PurE	N ⁵ -carboxyaminoimidazole ribonucleotide mutase
PurK	N ⁵ -carboxyaminoimidazole ribonucleotide synthase
RT-PCR	Real time polymerase chain reaction
SDS-PAGE	Sodium dodecyl sulfate polyacrylamid gel electrophoresis
SMILES	Simplified molecular-input line-entry system
SO	Sypro Orange
TB	Terrific broth
T _m	Boltzmann transition temperature
TRIS	Tris (hydroxy methyl) aminomethane
UIC	University of Illinois at Chicago

UV

Ultra violet

SUMMARY

Chapter 1 is an introduction to the project. It explains the concept of the approach as well as methods used to carry out the research plan.

Chapter 2 details of a high throughput screening of molecules binding to *BaPurE*, the docking methods, enzymatic assay and MIC measurements that resulted in the identification of 6 hit compounds with enzymatic inhibition and antimicrobial activity.

Chapter 3 is a study of solution properties of *BaPurE* in buffers of different ionic strength. Spectroscopical methods are employed to examine the molecular properties of *BaPurE* in solution.

Chapter 4 is a study of *BaPurE* unfolding with chemical denaturant Gdn-HCl or urea to further explain *BaPurE* confirmation in solution with different ionic strength.

CHAPTER 1

1 INTRODUCTION

1.1 Antibacterial Resistance

1.1.1 Resistance in Bacteria

Antibacterial drug has made its first appearance in medicine in the early 1900s with evidence of its usage tracing back to 350 - 550 CE. Antibacterial agents soon became one of the most successful methods to control infectious diseases in history of medicine (Aminov, 2010). Since the initial discovery of penicillin in 1928, the modern antibiotic era began with additional discovery of different classes of antibacterial agents. Common class of antibacterial agents are beta-lactams, macrolides, fluoroquinolones, tetracyclines and aminoglycosides. Currently, the rise of bacterial resistance to drugs has become a concern in medicine due to the ever-larger toll it takes on lives of infected people while delivery of new leads has become increasingly more difficult. Some of the resistant bacteria have become a concern including methicillin-resistant *Staphylococcus aureus* (MRSA). The need for a new class of antibiotic is an urgent issue that must overcome issues such as high cost of development and decreasing rate of discovery of new antibacterial agents.

1.1.2 Mechanism of Resistance

A spectrum of mechanisms are employed by the bacteria to develop antibiotic resistance trait. Some of the modes of resistance involve efflux pump where the bacteria pump the antibiotic agents outside the cell or a modified porin that prevents antibiotic agents from being taken up by the bacterial cell. Enzymatic inactivation of β -lactam by β -lactamase has also been

reported in antibiotic resistance (Nordmann *et al.*, 2012). Antibacterial resistance occurs when environment stressor is applied that selects for pre-existing drug-resistant trait. Discoverer of penicillin, Alexander Fleming, pointed out in his acceptance speech for the Nobel Prize in 1945 in physiology or medicine that high dosage is the key to treating bacterial infection. The logic in this was that if fewer bacteria remained after antibacterial drug treatment, the likelihood of the remaining bacteria to proliferate to develop resistance is low (Kupferschmidt, 2016).

1.2 *Bacillus anthracis*

B. anthracis is a Gram-positive pathogenic bacterium and is a primary biological warfare threat. Its spores were weaponized for aerosol delivery in 1991 during the Gulf War (Brook *et al.*, 2001) with a potential to become a tool of biological terrorism (Webb, 2003). Current treatment for *B. anthracis* infection is ciprofloxacin, a second-generation fluoroquinolone effective in treating both Gram-positive and Gram-negative bacterial infection (Karginov *et al.*, 2004). However, a number of clinical failure to achieve bacterial eradication using existing broad-spectrum fluoroquinolones such as ciprofloxacin was reported (Ball *et al.*, 2002), increasing the potential for development and spread of bacterial resistance. In the case of ciprofloxacin, treatment failure is due to the agent's poor activity against Gram-positive pathogens (Lee *et al.*, 1991). The need for a new antibacterial agent is evident.

1.2.1 *de novo* Purine Biosynthetic Pathway

For most organisms including *B. anthracis*, *de novo* purine biosynthetic pathway is an essential metabolic pathway (Zhang *et al.*, 2008) due to its critical up-regulation during *B. anthracis* infection when compared *in vitro* levels (Bergman *et al.*, 2007). Unlike the salvage pathway that recycles intermediates in the degradative pathway such as purine bases for

nucleotide synthesis, *de novo* purine pathway builds the purine base from conversion of 5'-phosphoribosyl pyrophosphate (PRPP) to inosine monophosphate (IMP) by use of cellular components (Zhang *et al.*, 2008). Importance of the *de novo* purine pathway has been demonstrated as being target for anticancer, antiviral and antibacterial drug development. The key difference of this pathway in eukaryotes (including human) and higher prokaryotes compared to lower prokaryotes (including *B. anthracis*) is the number of steps needed to complete the DNA base synthesis. As shown in Figure 1.1, in eukaryotic or higher prokaryotic organisms, the *de novo* pathway is carried out in ten steps by six enzymes (Zhang *et al.*, 2008). It was demonstrated recently that these enzymes can possibly form a large macromolecular cluster known as the 'purinosome' that function more effectively than individual enzymes (Zhao *et al.*, 2013; Chan *et al.*, 2015).

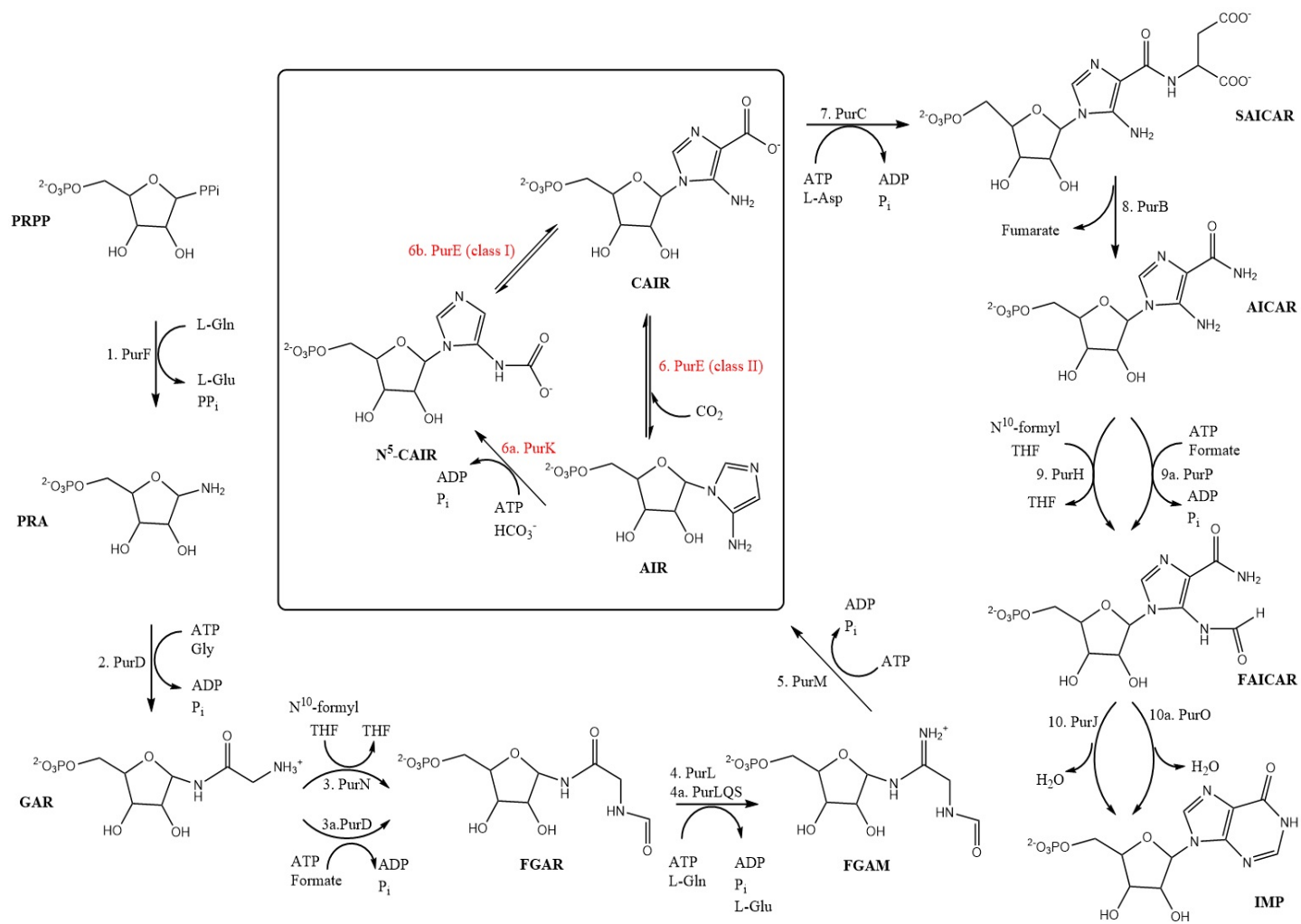


Figure 1.1. The *de novo* purine biosynthetic pathway.

1.2.2 Enzymes of Prokaryotic Purine Pathway

The major difference in eukaryotes and lower prokaryotes occurs in step six where 5-aminoimidazole ribonucleotide (AIR) is converted to 4-carboxy-5-aminoimidazole ribonucleotide (CAIR) (Figure 1.1). For this step, lower prokaryotic organisms use two enzymes, N⁵-carboxyaminoimidazole ribonucleotide mutase (PurE) and N⁵-carboxyaminoimidazole ribonucleotide synthase (PurK) while eukaryotic organisms uses carboxyaminoimidazole ribonucleotide synthase/succinoaminoimidazolecarboxamide ribonucleotide synthetase (Pur6) which is a bi-functional enzyme without creating the intermediate product N⁵-carboxyaminoimidazole ribonucleotide (N⁵-CAIR). It was revealed through a study that up-regulation of nucleotide synthesis during *B. anthracis* infection involve nine enzymes in the pathway (Samant *et al.*, 2008).

1.2.3 N⁵-Carboxyaminoimidazole Ribonucleotide Mutase

One of the nine essential enzymes in prokaryotic purine pathway was PurE, which showed significant reduction in *in vitro* growth of *B. anthracis* in human serum and did not show virulence to mice infected with *B. anthracis* with gene-knockout strain for PurE over a period of two weeks (Samant *et al.*, 2008). PurK catalyzes the conversion of AIR, ATP and HCO₃⁻ to N⁵-CAIR and PurE catalyzes the conversion of N⁵-CAIR to CAIR.

Crystal structure of N⁵-CAIR mutase from *B. anthracis* (BaPurE) is a homo-octamer constructed as a dimer of tetramers related perpendicular to a two-fold symmetry axis to the four-fold symmetry axis (Boyle *et al.*, 2005). A monomer consists of six α -helices that surround the five stranded β -sheet core (Protein Data Bank (PDB) code:1XMP). Substrate specificity of BaPurE and PurE domain of human Pur6 can be used to our advantage in designing an inhibitor

specifically for *BaPurE*. Active site residues of *BaPurE* were identified from the crystal structure of PurE from *Escherichia coli* (*EcPurE*) with a ligand nitroaminoimidazole ribonucleotide, NAIR (PDB code: 2ATE), and confirmed by mutant *BaPurE* studies (Firestine *et al.*, 2009).

1.2.4 Structure-Based Lead Design

In order to identify new antibacterial agents at a faster pace and at a reduced cost, structure-based design can be applied (Barker, 2006). The importance of PurE in purine pathway makes it a good druggable target to be considered in this approach. Since the structure of *BaPurE* was solved, a structure based lead design can be developed for lead molecule discovery (Anderson, 2003).

1.3 Biophysical and Biochemical Methods

1.3.1 Preparation of Recombinant Protein

Polymerase chain reaction (PCR) was used for inserting the gene of the target protein into a plasmid containing a LacZ promotor for isopropyl β -D-1-thiogalactopyranoside (IPTG) for induction of the protein expression (Christodoulou and Vorgias, 2002; Hansen *et al.*, 1998) in *E. coli* cells.

For purification of a recombinant fusion protein (protein fused with a tag), affinity chromatography can be used to accommodate either histidine (His) or glutathione S-transferase (GST) tag. His-tag (6 to 20 histidine residues) binds to resin with nickel charged nitrilotriacetic acid (Ni-NTA) ions while the impurities (other protein without the tag) are washed away, and the fusion protein is eluted by buffer with high (150 mM) imidazole concentration. GST tag (~26 kDa) in the fusion protein binds to glutathione (GSH) tagged resin while the impurities are washed away and eluted by 50 mM Tris (hydroxy methyl) aminomethane (TRIS) buffer with high

(5 mM) GSH concentration. Recombinant fusion protein obtained from column is cleaved by a serine protease via a protease site introduced between a linker and the target protein (Chang *et al.*, 1985) and separated from the tag by affinity column chromatography again. The purified protein can be passed through a size exclusion column to further remove impurities, if present.

1.3.2 Circular Dichroism

1.3.2.1 Far UV Region

Circular dichroism (CD) spectroscopy is a method that uses circularly polarized light to measure the difference in the absorption of the left-handed and right-handed polarized light by chiral molecules such as proteins due to its structural asymmetry (Greenfield, 2006). The signal that arise from the difference in absorption (or converted to ellipticity) can result in conformation dependent positive and negative signal while the absence of regular structure will result in no signal. From the CD signal, secondary structural elements of α -helices and β -sheets can be deduced or deconvoluted from its chromophore, peptide backbone, and the repeating geometry in the far-ultraviolet (UV) region between 190 - 250 nm (Pelton and McLean, 2000). Characteristic region for α -helices show minima at 208 and 222 nm, and for β -sheets, the minima appear at 214 - 218 nm depending on the amount of β -sheet structure. Ellipticity can be normalized to the number of peptide bonds in the protein as mean residue ellipticity (MRE) and to protein concentration. Percentage of α -helices and β -sheets content can be estimated from the normalized spectrum by various deconvolution algorithms include SELCON, VARSLC, CDSSTR, K2D and CONTIN (Kelly *et al.*, 2005).

1.3.2.2 Near UV Region

Chromophores of CD spectra in near-UV region (250 - 330 nm) are aromatic amino acid

residues such as tryptophan, tyrosine, phenylalanine and disulfide bond where each aromatic ring involves electron transition from a ground state with filled π orbital to an excited state with empty π^* orbital with higher energy (Strickland and Beychok, 1974). These aromatic chromophores have a plane of symmetry and are not considered optically active but they give near-UV CD signal through interacting with nearby groups of amino acid moiety and thus one can observe additional folding and/or twisting of secondary structural elements that form a tertiary structure which is the three dimensional conformation of protein structure.

Near-UV signals in 255 and 270 nm region are attributable to free amino acid residues and result in either positive or negative signal intensity that may vary dramatically. Residues that are immobile gives the strongest signal intensity. Residue phenylalanine and from 275 and 282 nm region to tyrosine and a peak near 290 nm region with fine structure between 290 to 205 nm region are attributable to tryptophan residue. Cystine residue (if any) is expected to show broad peaks above 240 nm and tends to begin at longer wavelength (>320 nm). Non-protein cofactors (if any) contribute by giving rise to broad weak signals throughout the near-UV region. CD signals in this region are weaker than those in the far-UV region. Lower molar extinction coefficient and lower number of the contributing chromophores are expected compared with far-UV region whose chromophores are peptide bonds (Kelly and Price, 2000). Other factors that influence near-UV CD spectra of aromatic residues include side chain interactions due to the rigidity of the protein. The environment of the aromatic side chains are reflected in the near-UV region, giving information about the tertiary structure of the protein (Kelly and Price, 2000). Inner core of most native proteins consist of more rigid or hydrophobic residues such as phenylalanine, tyrosine, and tryptophan. It is common for tyrosine and tryptophan residues to be

spatially close to each other, behaving as chromophores that are chirally perturbed, absorbing near-UV light that results in a characteristic bands in the spectrum. Although it is challenging to make assignment of these CD bands, its fine structure can potentially be a sensitive reporter of geometrical interaction between the phenol and indole rings of the tyrosine and tryptophan pair with a distinctive signal at 290 nm (Farkas *et al.*, 2016).

1.3.3 Denaturation

The extent of denaturation of a protein by a particular type of perturbation can be a measurement of its stability. Addition of temperature gradient or chemical agents such as urea or guanidine hydrochloride (Gdn-HCl) to a native protein will induce unfolding. The change from native state to unfolded state of the protein can be monitored by various spectroscopic methods.

1.3.3.1 Thermal Denaturation

Applying increasing levels of heat to a natively folded protein will disrupt hydrogen bonds and hydrophobic interactions that results in unfolding. The protein stability can be quantified by the value of a transition temperature (T_m) where half of the given protein becomes unfolded. Changes in T_m of a protein under two different conditions can provide information about the protein structure under these conditions (Kranz and Schalk-Hihi, 2011).

1.3.3.2 Chemical Denaturation

Chemical denaturants urea and Gdn-HCl interact with different part of the protein, causing certain parts of the protein to be exposed to the solvent, and thus unfolding the protein (Monera *et al.*, 1994). However, not all hydrophobic groups are buried and not all hydrophilic groups are exposed. Recently, it has been suggested that the protein surface stability can be changed by additives that manipulate the aqueous environment of the protein (von Hippel, 2016)

It has been demonstrated that the free energy of unfolding depends on denaturant concentration from which denaturant m-value can be derived (Myers *et al.*, 1995). The m-value show strong correlation with the difference between the amount of exposed surface area of a protein in its native and fully unfolded state. Thus, accessible surface area difference roughly equals to the size of the protein. The size related structural information can be obtained for proteins that undergo reversible two-state unfolding mechanism.

1.3.4 Size Exclusion Chromatography - Hydrodynamic Size

Protein in a solution may exhibit different oligomeric states (monomers, dimers, *etc.*). Hydrodynamic size of a protein may be obtained with a size exclusion column. A calibration curve of a semi-log plot of K_{av} and molecular mass of a set of proteins known to form monomers in solution, with $K_{av} = (\text{elution volume} - \text{void volume}) / (\text{total volume} - \text{void volume})$, can be used to determine the hydrodynamic molecular weight of a given protein. The void volume was measured by blue dextran (2000 kDa) for a given column, total volume was the geometric column volume calculated as $r^2 \cdot \pi \cdot \text{column height}$, and elution volume was for a given standard protein (other than blue dextran).

1.3.5 Assay

1.3.5.1 Thermal Shift Assay - Fluorescence

As discussed in section 1.3.3.1, stability of a protein can be estimated by temperature induced unfolding of a native state by calculation of T_m . One of the methods to measure T_m values was a fluorescent dye called Sypro Orange (SO) as a probe. Sypro Orange is hydrophobic, and when it in an aqueous environment, little fluorescent signal is detected. When a protein is in native state in a solution, Sypro Orange finds very few hydrophobic pockets on protein surface,

and exhibits little fluorescence signal. As the protein unfolds thermally, hydrophobic regions are exposed, and Sypro Orange selectively binds to them, resulting in increased emission signal. Stability of the protein can then be calculated by fitting the unfolding curve to obtain the temperature at where half of the protein is unfolded (T_m).

When the protein is stabilized through compound binding, the change in this protein stability upon binding the compound can be detected using this assay through a shift of T_m to a higher value (Lo *et al.*, 2004).

1.3.5.2 Assay for PurE Activity and Inhibition - UV Spectroscopy

As discussed in section 1.2.3, *BaPurE* catalyzes the conversion of N^5 -CAIR to CAIR, and *BaPurE* also catalyzes the conversion of CAIR to N^5 -CAIR. Due to instability of N^5 -CAIR, which decomposes to AIR, the conversion of CAIR to N^5 -CAIR is used to determine the enzyme activity. Absorbance maximum of CAIR overlaps with the absorbance maximum of N^5 -CAIR at around 253 nm (Meyer *et al.*, 1992). Thus, the disappearance of CAIR can be more accurately monitored at 260 nm where contribution of N^5 -CAIR is minimized (Meyer *et al.*, 1992). The initial rate of the disappearance of CAIR is monitored over a period of time where the relationship is linear.

Enzyme inhibition is monitored by addition of inhibitor compound in activity assay. When the inhibitor occupies available active sites and/or competes with substrate binding, the rate of disappearance of substrate is expected to decrease to indicate reduction of enzyme activity.

1.3.6 Tryptophan Fluorescence

Local conformation of a particular residue in a protein can be probed by fluorescence if

the residues emit fluorescent radiation such as the aromatic residues that absorb light followed by emission of light of a longer wavelength (Royer, 2006). Aromatic residues such as phenylalanine and tyrosine have lower extinction coefficient and quantum yield compared to tryptophan (Royer, 2006), making them less ideal for fluorescent excitation but useful nonetheless. Tryptophan residue fluorescence is sensitive to perturbation of its local environment (Vivian and Callis, 2001), and thus can be monitored exclusively even in the presence of phenylalanine and tyrosine residues, with excitation wavelength of 295 nm.

The maximum emission wavelength (λ_{max}) of tryptophan residue is correlated with the degree of solvent exposure to tryptophan. For example, 309 nm suggests hydrophilic environment where the residue is fully buried, 335 nm suggests that the residue is partially buried, and 355 nm suggests polar environment where the residue is fully exposed (Royer, 2006). The signal intensity from tryptophan also provides information on the polarity of local environment. The intensity is reduced upon exposure to water or other quenching molecules such as acrylamide or potassium iodide (KI). These molecules are known to interact with the excited chromophore and yields a product that decays via a non-radiative pathway that results in a diminished fluorescence signal (Moller and Denicola., 2002). The accessibility of a tryptophan residue to the added quenchers is used to probe the location of the tryptophan residue which may reflect the flexibility of a protein molecule. Stern-Volmer constant (K_{SV}) for rate of quenching can be determined by measuring the fluorescence intensity or the fluorescence life time as a function of quencher concentration from the Stern-Volmer plot (Strambini and Gonnelli, 2010). *BaPurE* has a single tryptophan residue per monomer (eight per octamer) that is well exposed to the solvent, according to its x-ray structure.

1.3.7 High Throughput Screening

High throughput screening (HTS) method screens for molecules that inhibit the activity of an enzyme or that bind an enzyme. The molecules to be screened are in a chemical library. A 384-well plate is usually used to carry out the screening reaction. One of the method to screen for compounds binding to an enzyme is to detect the increase of T_m due to enzyme stabilization by compound binding. A real time-PCR (RT-PCR) instrument provides accurate and steady temperature increase and monitors fluorescence intensity at various wavelength. The experimental data are analyzed by a program associated with the instrument to give the T_m values of each samples in the wells of the 384-well plate.

The quality of the HTS is assessed by Z' -factor calculation (Zhang *et al.*, 1999). Z' -factor between 0.5 to 1.0 is expected for reliable assays and 1.0 for a perfect assay (Zhang *et al.*, 1999). Variability in average values examined by evaluating the HTS assay quality. Screening window coefficient Z' -factor was determined between the positive and negative control as an indicator of signal and background separation (Macarron and Hertzberg, 2009).

CHAPTER 2

A HIGH THROUGHPUT SCREENING FOR INHIBITORS OF PURE FROM *BACILLUS ANTHRACIS*

Identification of *Bacillus anthracis* PurE Inhibitors with Antimicrobial Activity. Anna Kim[†], Nina M. Wolf[†], Tian Zhu, Michael E. Johnson, Jiangping Deng, James L. Cook, Leslie W.-M. Fung. *Bioorganic & Medicinal Chemistry* 23 (2015) 1492-1499.

[†] These two authors contributed equally.

*My contribution to this paper is described in this chapter.

The full article is presented in Appendix A

2.1 Introduction

The rise of antibacterial drug resistance is currently at an alarming rate. The rate of discovery for new antibacterial agent is on the decline, and, of the drugs that are in development, bacteria have developed resistance before they even reached the market (Kupferschmidt, 2016). Discovery of new antibacterial agent for critical pathway in bacterial metabolism is needed (Murima *et al.*, 2014). Importance of purine biosynthetic path for bacterial virulence in infected host has been demonstrated (Bergman *et al.*, 2007) and especially the dependence of virulence on the steps involving the enzyme PurE (Samant *et al.*, 2008). Despite the structural and sequence

similarity between bacterial PurE and eukaryotic PurE domain of Pur6, each enzyme show high specificity for its own substrates which makes PurE a good target for inhibitor design.

In this chapter, a HTS thermal shift assay using SO fluorescent probe was employed for recombinant *BaPurE* to identify molecules that bind to the enzyme (Fung group: AJ and Nina M. Wolf). Hits from the screening were further selected by structure based *in silico* docking (Johnson group: Tian Zhu) and by enzyme inhibition assay (Fung group: Anna K. Jones). Minimum inhibition concentrations (MIC) were determined for compounds that were found to bind and inhibit the enzyme (Cook group: Jiangping Deng). MIC values were obtained against *B. anthracis* (Δ ANR strain), *E. coli* Δ TolC⁻ (BW25113 strain), *S. Aureus* for both methicillin susceptible strain (MSSA) and methicillin resistant strain (MRSA), *F. tularensis* and for *Y. Pestis*. A common core structure, 1-carboxyamido-1,3,4-oxadiazole, was found for compounds with MIC values of 0.5 - 0.15 μ g/mL against *B. anthracis* (Fung group: Anna K. Jones).

2.2 Experimental Procedures

2.2.1 Sample Preparation

(Fung group, AJ and Nina M. Wolf)

Recombinant *BaPurE* was prepared by Nina M. Wolf (Fung group). pDEST15-*BaPurE* vector containing ampicillin resistant gene, *BaPurE* gene (BA0288) from *B. anthracis* (Δ ANR) tagged with GST with a linker containing the thrombin cleavage site (sequence: PWSNQTSLYKKAGSLVPRGSH) was expressed in GST-*BaPurE* *E. coli* BL21c⁺ cells. The overnight cell culture was initially grown in 50 mL of Luria broth (LB) medium at 37 °C and was transferred to a fermentor instrument (Bioflo 110, New Brunswick, Enfield, CT) with 2 L of Terrific broth (TB) medium with 0.3 mM ampicillin. Cells were grown for 3 hours at 37 °C and

was induced with 1 mM IPTG at reduced temperature (25 °C) for 3 hours. Nonionic surfactant was added to cell followed by sonication and centrifugation to give cell lysate. GST-PurE fusion protein was purified from the cell lysate by a glutathione affinity column (Sigma-Aldrich) in phosphate (5 mM) buffered saline pH 7.4 with 150 mM NaCl (PBS). For the elution of the fusion protein, fresh 5 mM GSH in 50 mM TRIS buffer at pH 8.0 was used. Bovine thrombin at concentration of 1 unit per 1mg fusion protein was used to cut the fusion protein. *BaPurE* was purified from the GST-tag and/or any uncleaved fusion protein by the affinity column and was stored in PBS at -80 °C. Purity of *BaPurE* sample was determined by sodium dodecyl sulfate polyacrylamid gel (16%) electrophoresis (SDS-PAGE). The prepared protein was confirmed as *BaPurE* by mass spectrometry at the DNA Services Facility at Research Resources Center, University of Illinois at Chicago (UIC) and by activity assay. All thawed samples underwent centrifugation (Sorvall Legend RT at 3400xg for 2 minutes) before usage.

2.2.2 Thermal Unfolding Assay with Positive Control

(Fung group, AJ and Nina M. Wolf)

BaPurE (10 µM) in 25 mM or 50 mM TRIS aminomethane buffer (prepared by overnight dialysis at 4 °C with 1:500 protein to buffer ratio) at pH 8.0 with no NaCl (25TRIS8-0 or 50TRIS8-0) was thermally unfolded from 25 to 70 °C in the presence of 5X Sypro Orange (Invitrogen, Carlsbad, CA) prepared from 5000X stock solution in anhydrous dimethylsulfoxide (DMSO). Conductivity and pH of the buffer were measured using a conductivity probe (YSI 3417) and a pH probe (Thermo Fisher Scientific), respectively. Change in Sypro Orange fluorescence over a temperature gradient was monitored with a fluorescence spectrometer (Jasco FP-6200) with excitation wavelength of 490 nm and emission wavelength of 563 nm. NAIR, an

inhibitor of PurE, was used as a positive control (at 10 mM concentration) to verify the binding induced stability in *BaPurE* both 25TRIS8-0 or 50TRIS8-0 buffer.

T_m was determined by Boltzmann fit, assuming two state function. The fit was made from the lowest fluorescence intensity baseline to the highest fluorescence intensity between around 45 to 55 °C.

2.2.3 High Throughput Screening by RT-PCR

(Fung group, AJ and Nina M. Wolf)

Multiple batches of *BaPurE* samples were combined (about 100 mg) and dialyzed for 16 hours at 4 °C in 25TRIS8-0. 24,917 compounds in DMSO (10 mM stock) from a chemical library (Life Chemicals, Burlington, Canada) were delivered with other components of the assay to the wells in the 384-well white plate (Abgene SuperPlate, Fisher Thermo Scientific) by a liquid handling system (Freedom Evo, Team, Mannedorf, Germany) at the HTS facility at UIC. Each plate, prepared as a batch of 10 or 20, was sealed by plastic films (Applied Biosystems, Foster City, CA) to prevent solvent evaporation and was stored at 4 °C between sample preparation and thermal denaturation to run, which was between 10 to 30 minutes. Total of 156 plates for the library compounds in duplicate plus control samples in about 60,000 wells were run by Fung group (AJ and Nina M. Wolf) on RT-PCR instrument (ViiA7, Applied Biosystems, Carlsbad, CA). NAIR was used as the positive control. Wells with just Sypro Orange provided background fluorescence signal and *BaPurE*, Sypro Orange with 1% DMSO were used as control. Optimal excitation wavelength as well as instrument fluorescent filter settings for the RT-PCR instrument was determined by Nina M. Wolf. Filter x1 (470 ± 15) and emission filter m2 (558 ± 12) was used to monitor the change in the 5X Sypro Orange signal over a temperature

range of 25 to 95 °C at a temperature increase rate of 0.075 °C/s. The entire run time per plate was about 20 minutes.

2.2.4 Hit Selection and Assay Evaluation

(Fung group, AJ with Nina Wolf)

Experimental data were analyzed by the Protein Thermal Shift Software (Applied Biosystems) to give Boltzmann transition temperature (T_m) of each unfolding profile. ΔT_m was calculated for each compound based on its deviation from control T_m ($\Delta T_m = T_m$ with compound - T_m without compound). Compounds that were eliminated first were those ΔT_m values between duplicate runs were greater than 1.0 °C. Hit compounds were those whose ΔT_m was between 1.0 to 20.0 °C, a range of thermal shift values suggested by literature (Ferguson *et al.*, 2011; Sainsbury *et al.*, 2011; Sun *et al.*, 2011).

Z' -factor was determined (See also 1.3.7) to assess the quality of the HTS. The following equation was used for Z' -factor calculation: $Z' = 1 - (3 \sigma_{C+} + 3 \sigma_{C-}) / |\mu_{C+} - \mu_{C-}|$ where the average T_m value (μ_{C+}) and its standard deviation (σ_{C+}) were calculated from wells containing NAIR, a known inhibitor of *BaPurE* (thus it binds to *BaPurE*). The average T_m value (μ_{C-}) and its standard deviation (σ_{C-}) without NAIR.

2.2.5 In Silico Screening

(Johnson group, by Tian Zhu)

The hit compounds were further screened by structure based *in silico* active site docking by first preparing 3D structural of each hit compound (using LigPrep, Schrödinger) to its most energetically and structurally favorable conformation from the “simplified molecular-input line-entry system” (SMILES) strings. Active site information was obtained from published

structure of PurE (*EcPurE*) with a ligand (PDB: 1D7A). GOLD v5.0.1 (Cambridge Crystallographic Data Centre; Cambridge, United Kingdom) was used to dock the converted compound structures to the active site of the *EcPurE* where the ligand, AIR, is bound. Size of the active site was defined with a binding site sphere with radius of 10 Å centered around AIR.

2.2.6 Enzyme Activity and Inhibition Assay

Enzymatic activity of *BaPurE* was obtained by monitoring the reverse conversion of CAIR to N⁵-CAIR by *BaPurE* (Meyer *et al.*, 1992; Tranchimand *et al.*, 2011). Enzyme activity was determined from the rate of disappearance of substrate CAIR in $\Delta A_{260}/\Delta t$. The rate was converted to specific activity using the extinction coefficient of CAIR, 8930 M⁻¹ cm⁻¹. Specific activity determined in literature reported the extinction coefficient of CAIR as 10500 M⁻¹ cm⁻¹ and reduced it to 8930 M⁻¹ cm⁻¹ to account for the appearance of N⁵-CAIR in the enzymatic reaction (Constantine *et al.*, 2006). The absorbance of CAIR was monitored using a UV-Vis spectrophotometer (Genesys10).

The activity of 10 nM *BaPurE* in 25TRIS8-0 plus 1% DMSO (to be consistent with compound inhibition activity measurements with the compound stocks being in DMSO) with substrate CAIR (29 µM) was obtained from the absorbance of CAIR at 260 nm (A_{260}) as a function of time for every 5 seconds for 1.5 min to give the linear portion of the data (slope = initial rate). *BaPurE* inhibition activity was determined by introducing a known inhibitor NAIR (10 µM final concentration) to the assay to be compared to *BaPurE* activity in absence of NAIR. To determine the activity with a given compound, *BaPurE* was incubated with the compound for 1.5 min prior to the addition of CAIR. Inhibition activity was determined with the following equation: % inhibition = $100 - (\text{Rate}_{\text{compound}} / \text{Rate}_{\text{BaPurE}} \times 100)$

Inhibition activity results of 79 compounds in DMSO with constant A_{260} readings (at 10 μM) in the absence of enzyme were used. Enzyme inhibition activity was tested at compound concentrations of: 50 μM , 20 μM , and 10 μM . *BaPurE* (20 nM) and each compound (20 μM) was incubated at 20 °C for 1.5 minutes to maximize enzyme exposure to the compound before addition of equal volume of CAIR (final concentration for *BaPurE* was 10 nM, CAIR was 30 μM , compound was 10 μM with 1% DMSO) to start the assay.

2.2.7 Minimum Inhibitory Concentration

(Cook group, by Jiangping Deng)

Minimum inhibitory concentration (MIC) values of the hit compounds were determined. A commercial antibiotic, ciprofloxacin was used as a positive control for this study.

2.3 Results

2.3.1 Dependence of ΔT_m on Ionic Strength

The unfolding profile of *BaPurE* in Figure 2.1 show decrease in fluorescence intensity until sharp increase was seen between 45 - 50 °C followed by another decrease past 50 °C. The initial decrease in fluorescence intensity was less pronounced (as shown in Figure 2.1) with stock SO that underwent less (less than 3 times) freeze-thaw cycle. The difference in T_m of *BaPurE* in 25TRIS8-0 (1200 μMHO) and 50TRIS8-0 (2600 μMHO) was 4.9 °C (Figure 2.1).

Thermal unfolding of *BaPurE* with NAIR (10 mM) was monitored in the two buffer conditions (25TRIS8-0 or 50TRIS8-0). Conductivity of 25TRIS8-0 was 1300 μMHO and 50TRIS8-0 was 2600 μMHO . The T_m shifted in 25TRIS8-0 with binding of NAIR was by 5.0 °C in 25TRIS8-0 and 1.0 °C in 50TRIS8-0 buffer (Figure 2.2). Signal from fluorescence of NAIR and 5X SO did not interfere with the fluorescence signal of *BaPurE* unfolding.

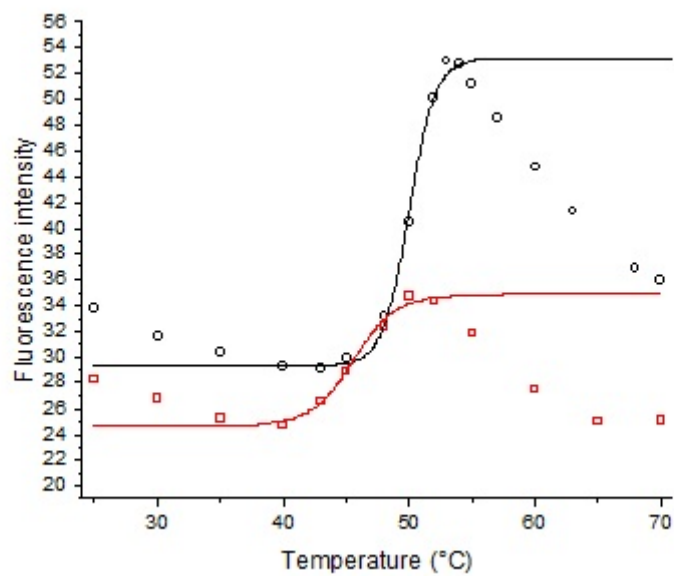


Figure 2.1. Thermal unfolding of 10 μ M *BaPurE* in 25TRIS8-0 (□) or 50TRIS8-0 buffer (○) using 5X Sypro Orange as a probe with excitation at 490 nm and monitoring the fluorescence intensity at 563 nm. T_m in 25TRIS8-0 = 45.7 $^{\circ}$ C, T_m in 50TRIS8-0 = 50.6 $^{\circ}$ C.

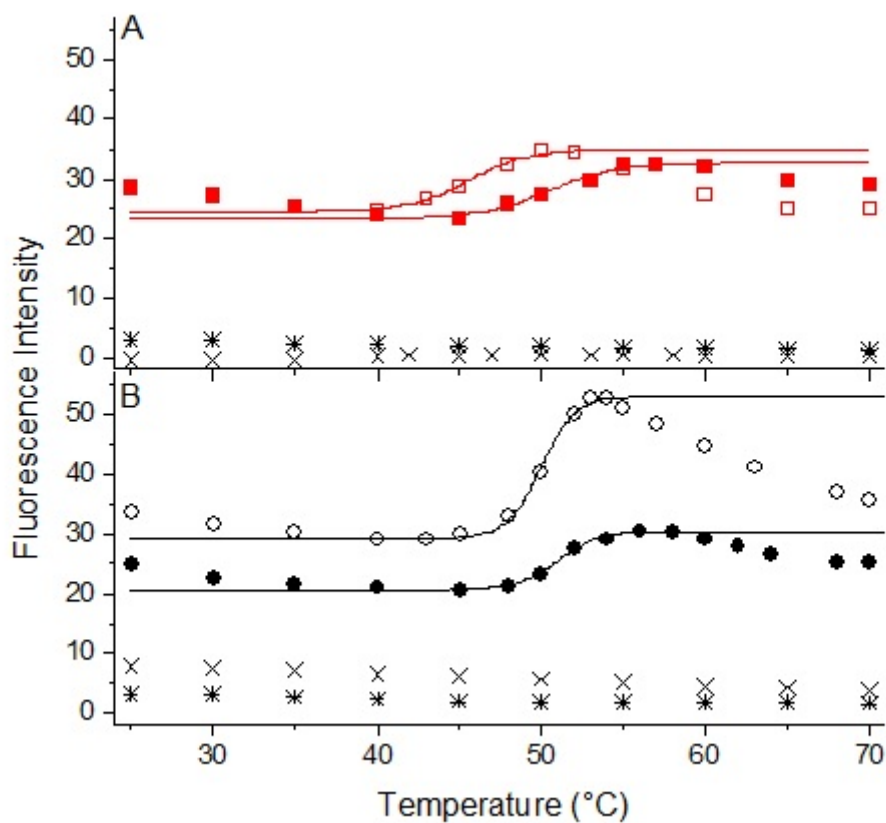


Figure 2.2. Thermal unfolding of 10 μ M *BaPurE* in 25TRIS8-0 or 50TRIS8-0 buffer using 5X Sypro Orange as a probe with excitation at 490 nm and monitoring the fluorescence intensity at 563 nm. (A) T_m in 25TRIS8-0 (\square) = 45.6 $^{\circ}$ C, with 10 mM NAIR (\blacksquare) = 50.6 $^{\circ}$ C (B) T_m in 50TRIS8-0 (\circ) = 50.0 $^{\circ}$ C, with 10 mM NAIR (\bullet) = 51.0 $^{\circ}$ C. Fluorescence intensity without *BaPurE* (\times) and only 5X SO ($*$) was monitored for signal interference.

2.3.2 Hit selection and Z'-Factor for Assay Reliability

The average T_m value on the plates without NAIR was $47.8\text{ }^{\circ}\text{C}$ (μ_{C-}) with a standard deviation of $0.3\text{ }^{\circ}\text{C}$ (σ_{C-}) ($n = 32$ across 2 plates), and with NAIR (10 mM) was $53.4\text{ }^{\circ}\text{C}$ (μ_{C+}) with a standard deviation (σ_{C+}) of $0.5\text{ }^{\circ}\text{C}$ ($n = 32$ across 2 plates). Z' -factor was 0.56.

The average T_m value *BaPurE* without compound (control) was $47.6 \pm 0.6\text{ }^{\circ}\text{C}$ ($n = 4499$ across 156 plates). 525 thermal shift hits were identified by ΔT_m analysis which was further narrowed down by molecular docking selection. GOLD docking scores assigned to docking of known substrate and inhibitor, CAIR and NAIR respectively, to the active site yielded 55 for both molecules. Compounds with docking scores greater than or equal to 55 were selected from docking analysis, yielding 79 compounds.

2.3.3 Inhibition Activity

A typical enzymatic activity of 10 nM *BaPurE* in 25TRIS8-0 was shown in Figure 2.3. The initial rate of 10 nM *BaPurE* in 25TRIS8-0 was calculated from the linear portion of the negative slope of the substrate concentration (A_{260}) versus time. Enzymatic activity of 10 nM *BaPurE* in 25TRIS8-0 was $0.0086 \pm 0.0028\text{ }A_{260}/\text{min}$ ($n = 100$).

The average activity of *BaPurE* with 15 compounds (at 10 μM , several compounds showed precipitation at 100 μM concentration) with inhibition was $0.0073 \pm 0.00197\text{ }A_{260}/\text{min}$ ($n = 37$) with an average inhibition of 15%. A run of activity of *BaPurE* with and without compound LC1 is shown in Figure 2.3. The rate with LC1 was $-0.0077\text{ }A_{260}/\text{min}$ and without LC1 was $-0.0109\text{ }A_{260}/\text{min}$. Inhibition of LC1 was 29% determined from the ratio of slope of reaction with and without LC1. Total of 79 compounds were tested for *BaPurE* inhibition, 65 compounds showed no inhibition. Table 2.1 showed individual % inhibition of each compound

determined by using individual control pair values.

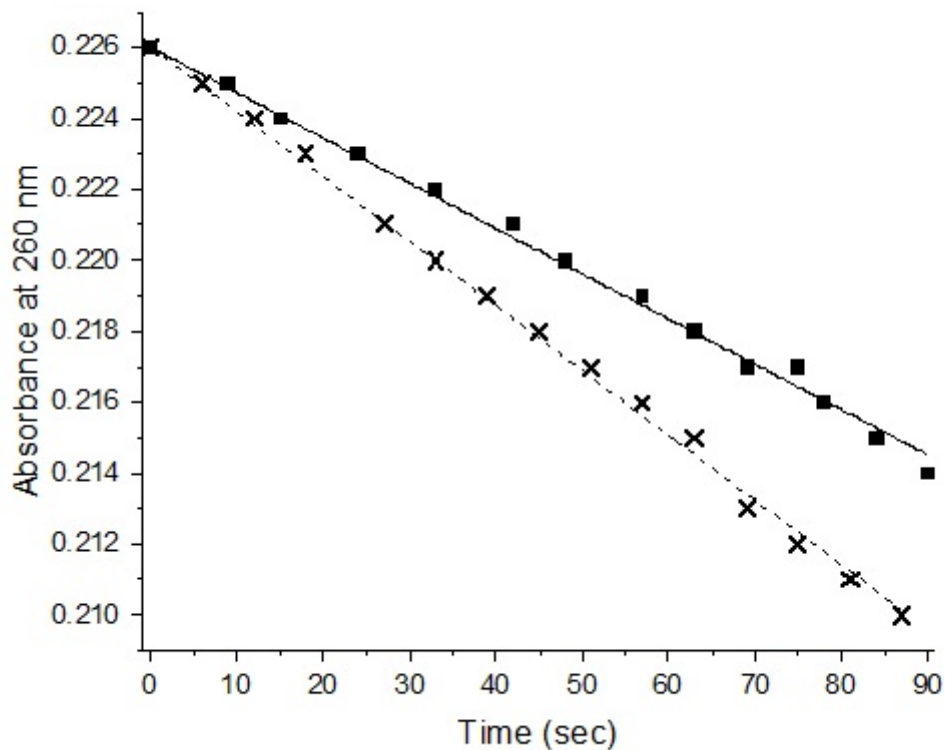


Figure 2.3. Activity of 10 nM *BaPurE* in 25TRIS8-0 (1300 μ MHO) was monitored by UV-Vis spectroscopy at 260 nm for monitoring the disappearance of substrate CAIR (30 μ M). Enzyme activity was monitored by incubating *BaPurE* with compound LC1 (■) or with 1% DMSO (×) for 1.5 minutes at 20 °C before addition of CAIR. The rate with LC1 was $-0.0077 A_{260}/\text{min}$ and without LC1 was $-0.0109 A_{260}/\text{min}$. Inhibition of LC1 was 29% determined from the ratio of slope of reaction with LC1 and without LC1 expressed as percentage.

Table 2.1. Inhibition of *BaPurE* by hit compounds from HTS.

Cpd Code	Rate with cpd (A260/min)								Rate without cpd (A260/min) ^a			Avg inh (%)
	Run1	Run2	Run3	Run4	Run5	Run6	Avg	SD	Avg	SD	n	
LC1	0.0072	0.0066	0.0066	0.0052	0.0073	0.0052	0.0064	0.00084	0.0087	0.00066	10	27
LC2	0.0070	0.0075					0.0073	0.00035	0.0090	0.00109	10	19
LC3	0.0062	0.0042	0.0065				0.0056	0.00125	0.0065	0.00042	8	13
LC4	0.0041	0.0041					0.0041	0.00000	0.0051	0.00058	8	19
LC5	0.0055	0.0049					0.0052	0.00042	0.0065	0.00057	4	20
LC6	0.0044	0.0078					0.0061	0.00240	0.0072	0.00205	5	15
LC7	0.0070						0.0070	N/A	0.0097	0.00085	4	28
LC8	0.0088	0.0098					0.0093	0.00071	0.0116	0.00196	6	20
LC9	0.0088	0.0083	0.0099				0.0090	0.00082	0.0109	0.00118	5	17
LC10	0.0087	0.0081					0.0084	0.00042	0.0102	0.00072	5	17
LC11	0.0074						0.0074	N/A	0.0086	0.00032	3	14
LC12	0.0049	0.0082	0.0045				0.0059	0.00203	0.0067	0.00153	3	12
LC13	0.0092	0.0102	0.0097				0.0097	0.00050	0.0109	0.00118	5	11
LC14	0.0097	0.0099					0.0098	0.00014	0.0105	0.00085	3	7
LC15	0.0105	0.0086	0.0086				0.0092	0.00110	0.0098	0.00110	6	6

^aValues were averages, specific to the individual run with each compound.

2.3.4 Minimum Inhibitory Concentration

MIC values of compound LC1 - LC5 against *B. anthracis* were 0.05 to 0.15 µg/mL. The rest of the tested compounds showed larger (>12.5 µg/mL) MIC values against *B. anthracis*, *F. Tularensis* and *Y. Pestis*. A summary of HTS of BaPurE for inhibitors is shown in Figure 2.4.

2.3.5 Identification of a Core Structure

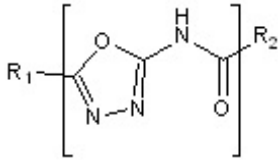
Among the six of the fifteen tested compounds with low MIC values (0.05 to 0.78 µg/mL), a common core structure, a 2-carboxamido-1,3,4-oxadiazole, was identified (Table 2.2). The most common R₁ group structure is 2,5-dichlorobenzene.

Table 2.2. The thermal shift (ΔT_m) of *BaPurE* induced by compounds (100 μ M) and inhibitory activity of compounds (10 μ M) toward *BaPurE* in 25 mM TRIS buffer. Also listed are the MIC values of the compounds against various bacterial strains.

Compound	ΔT_m (°C) ^a	Inhibition (%) ^b	MIC (μ G/mL)					
	<i>BaPurE</i>	<i>BaPurE</i>	<i>Ba</i> ^c	<i>Ft</i> ^c	<i>Yp</i> ^c	<i>MSSA</i> ^c	<i>MRSA</i> ^c	<i>Ec</i> Δ <i>TolC</i> ^c
LC1	2.0	27	0.15	6.25	> 12.5	0.29	0.39	0.29
LC2	7.9	19	0.10	3.1	> 12.5	> 12.5	6.25	0.39
LC3	1.9	13	0.10	> 12.5	> 12.5	> 12.5	> 12.5	> 12.5
LC4	2.4	19	0.10	6.3	> 12.5	0.2	> 12.5	0.02
LC5	1.1	20	0.05	1.6	3.1	0.78	1.95	0.07
LC6	1.4	15	0.78	1.2	3.1	1.56	3.13	0.39
NAIR	5.4	24	ND	ND	ND	ND	ND	ND
Ciprofloxacin	ND ^d	ND	0.11	0.03	0.04	0.35	0.34	0.01
Linezolid	ND	ND	2 ^e	32 ^f	ND	2 ^g	ND	ND

^a $\Delta T_m = T_m^{Ec} - T_m^E$, with the average transition temperature for *BaPurE* (T_m^E) as 47.6 °C from high throughput screening, with n = 4878. T_m^{Ec} values were average values from replicate runs in high-throughput screening. For NAIR, n = 32. ^bValues were averages, with n = 2 - 4 with the standard deviations ~ 7%. ^c*Ba* = *B. anthracis* (Δ ANR strain) cells; *Ft* = *F. tularensis* cells; *Yp* = *Y. pestis* cells; *MSSA* = *S. aureus* (methicillin susceptible strain 29213) cells; *MRSA* = *S. aureus* (methicillin-resistant strain 43300) cells; *Ec* Δ *TolC* = *E. coli* (BW25113 Δ *TolC*) cells. ^dND = not determined. ^eHenver *et al.*, 2012. ^fRamados *et al.*, 2013. ^gKreizinger *et al.*, 2013.

Table 2.3. The structures of the inhibitor compounds in Table 1. These compounds include a core structure of 2-carboxamido-1,3,4-oxadiazole, with various R₁ and R₂ groups.

		
Compound	R ₁	R ₂
LC1	thiophene	1-(toluene-4-sulfonyl)-1,2,3,4-tetrahydro-quinoline
LC2	2,5-Dichlorobenzene	2-Phenyllepidine
LC3	2,4-Dimethylbenzene	Benzophenone
LC4	2,5-Dimethylbenzene	3-Chlorobenzene
LC5	2,5-Dimethylbenzene	2,5-Chlorothiophene
LC6	4-Bromobenzene	4-Chloroanisole

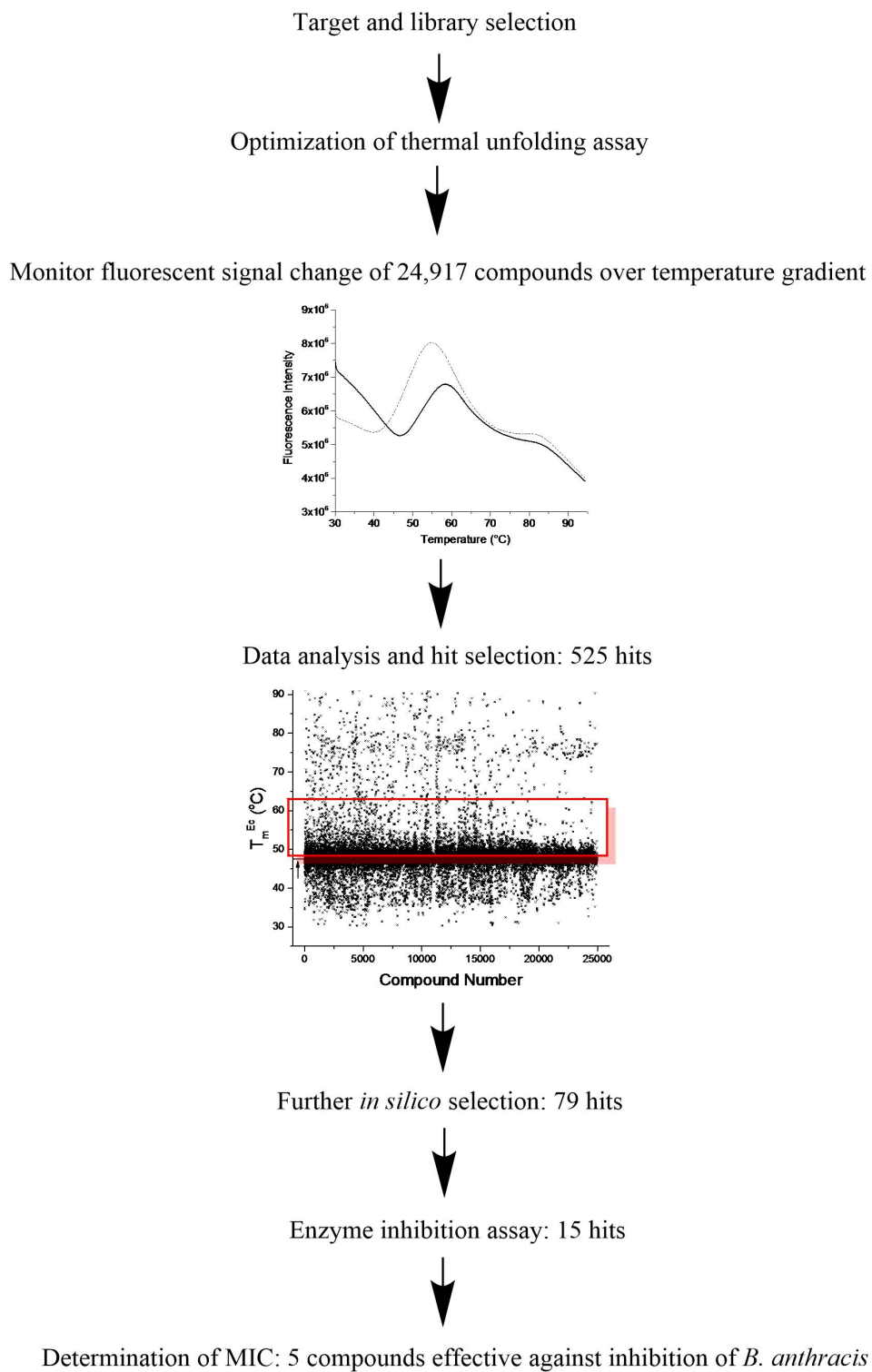


Figure 2.4. A summary of HTS of *BaPurE* for inhibitors.

2.4 Discussion

In many pathogens, including *B. anthracis*, N5-carboxyaminoimidazoleribonucleotide mutase (PurE) plays a key role as an essential enzyme in the *de novo* purine biosynthetic pathway (Samant *et al.*, 2008). In this project, recombinant *BaPurE* was targeted to identify small compounds that inhibit the enzymatic activity as well as reduce the growth of *B. anthracis*.

Thermal shift assay was used in high-throughput screening since the UV-based enzyme assay method (Meyer *et al.*, 1992; Tranchimand *et al.*, 2011) is insensitive for HTS. It was demonstrated that larger thermal shift caused by a known inhibitor NAIR in lower ionic strength buffer such as 25TRIS8-0 compared to higher conductivity buffer such as 50TRIS8-0. *BaPurE* in 25TRIS8-0 was less stable than in 50TRIS8-0 by 5.0 °C, but exhibited a larger stabilization by binding NAIR by 4.0 °C. To increase the detection of sensitivity of compound binding, 25TRIS8-0 was chosen as the buffer to be used in the HTS. Out of about 25,000 compounds, approximately 500 compounds were identified as hits (as binding to *BaPurE*) in HTS with 25TRIS8-0 buffer. These compounds were further selected for their likelihood to bind to the active site of *BaPurE*. Z'-factor of 0.56 indicated that this was a reliable assay according to the suggested value range discussed in section 1.3.7.

For enzyme inhibition activity assay, compound precipitation was observed (at 100 µM, same concentration as the HTS) and the compound signal interfered with the UV-signal which made the assay less reliable. Enzyme inhibition activity was tested with lowered compound concentrations than the HTS due to solubility issues at concentrations of 50, 20, and 10 µM. The assay carried out at 10 µM compound concentration appeared to be most soluble (no visible precipitation) with minimal interference in the UV-signal from the compound. *BaPurE* (20 nM)

and each compound (20 μ M) was incubated at 20 °C for 1.5 minutes to allow some time for enzyme exposure to the compound for binding reaction before addition of equal volume of CAIR. The final volume of the enzyme inhibition activity assay had to be increased due to the insensitivity of the UV-Vis method to detect CAIR disappearance. The HTS condition (lowered compound concentration, compound-enzyme incubation time, increase in assay volume) was not replicated in the enzyme inhibition activity assay but the modification of such conditions still provided valuable information regarding inhibition activity of the compound to the *BaPurE* enzyme.

The inhibition shown by the 15 compounds was between 10 - 20% , which is relatively low (Table 2.1). This is possibly due to lowered compound concentration (10 μ M) compared to the HTS. Previously identified inhibitor NAIR has been reported as a steady-state inhibitor of *ecPurE* with K_i of 0.5 μ M as well as *Gallus gallus* Pur6 with K_i of 0.34 μ M (Firestine *et al.*, 1994). NAIR was not considered as a drug candidate because it was reported to be an inhibitor for both *Gallus gallus* AIR carboxylase and PurE, and, it was shown to be a better inhibitor of AIR carboxylase than PurE.

Compounds that showed enzyme inhibition were tested for antimicrobial activity against *B. anthracis* and other pathogens such as *E. coli* (BW25113 strain, wild-type and TolC⁻), *S. aureus* for both methicillin-susceptible *S. aureus* (MSSA) and methicillin-resistant strain (MRSA), *F. tularensis* and *Y. Pestis*. MICs of the 15 compounds tested against five virulent pathogens including *B. anthracis* and the results were summarized in Table 2.2 (Kim *et al.*, 2015). Certain compounds showed cross-strain activity against *F. tularensis* and *Y. Pestis* but the MIC values were ten times greater than values for *B. anthracis*. Limited cell penetration or

differential efflux can be potential cause for the observed reduction in activity in these species. Cross-strain activity was observed against *S. aureus* with MIC < 1 µg/mL which suggest that such compounds may represent a new class of antimicrobial agents against MRSA. This finding can be important for expanding the clinical options for MRSA infections.

Concentration of compound needed for enzyme inhibition is much higher than MIC values which suggest that other cellular proteins or enzymes may also be targeted by these compounds.

A common core structure, 1-carboxyamido-1,3,4-oxadiazole, was found for compounds with low MIC values against *B. anthracis*. In another study, isatin core structure were found to be inhibitors of N⁵-CAIR synthetase and that structural modification of the core resulted in different inhibitory effects (Firestine *et al.*, 2009). Modification of the oxadiazole core structure can be made to improve the potency of *BaPurE* inhibitors.

2.5 Conclusion

Thermal shift assay was optimized for HTS with reliable validation method (Z'-factor of 0.57). The assay identified 2% of the library of about 25,000 compounds as hits which were further selected by *in silico* docking and enzyme activity assay as well as antimicrobial activity against *B. anthracis* along with other pathogenic strains. Six compounds that share an oxadiazole core structure was identified with low MIC values relative to ciprofloxacin with potential to be promising antimicrobial agents against *B. anthracis* as well as MRSA.

CHAPTER 3

SOLUTION PROPERTIES OF *BAPURE* AND BIOCHEMICAL AND BIOPHYSICAL CHARACTERIZATION

*A collaborative work with Nina M. Wolf where my contribution to this project is described in this chapter

3.1 Introduction

To combat the increasing problem of drug resistance in medicine today, the search for drug molecules that are specific to such infectious organisms are needed. Organisms that have been used for bioterrorism, such as *B. anthracis*, are of special concern (Missiakas and Schneewind, 2005).

X-ray crystal structure of PurE from *B. anthracis* is available in PDB which can be aligned with that of PurE from *E. coli* with a ligand to extract information regarding the active site. *BaPurE* has 8 active sites in its homo-octomeric form where each of the active site is created by three monomers. From the previous chapter, *BaPurE* exhibits different thermal stability upon binding a ligand in buffers with different ionic strength, which suggests that *BaPurE* is in different conformation under the two different conditions. Protein motion between different conformational states has been ignored in many drug design when protein flexibility is key to understanding biological effects exerted by drug molecules (Teague, 2003). The differences in *BaPurE* conformations in different ionic strength can be explored to better understand conformational stability for better drug design for this essential enzyme in purine

biosynthesis pathway (Samant *et al.*, 2008).

The local conformation of *BaPurE* in different buffer condition with various ionic strength was studied by monitoring the secondary and tertiary structure for α -helices content and conformational orientation of aromatic amino acid residues. Taking advantage of the single tryptophan residue which is a sensitive probe to monitor environment polarity in *BaPurE* monomer, fluorescence spectroscopy was employed to monitor changes in response to protein conformational transitions from one ionic strength condition to another. Further structural information can be observed by tryptophan quenching by addition of quencher molecules to probe the accessibility of the tryptophan residue to the quencher. Tryptophan can be quenched by a neutral quencher molecule acrylamide to probe the polarity of the environment around the residue. When excited, tryptophan residues in protein react with external quencher molecules to produce an excited product that undergoes non-radiative pathway decay or dynamic quenching process (Moller and Denicola, 2002). The change in tryptophan fluorescence intensity due to the presence of acrylamide is expressed by the Stern-Volmer equation which gives information about accessibility of acrylamide to tryptophan residue (Moller and Denicola, 2002).

3.2 Experimental Procedures

3.2.1 Protein Preparation

See 2.2.1. for elution of the fusion protein, except with a lower GSH concentration (1.5 mM) to give a higher fusion protein purity (90% or greater, as determined by SDS-PAGE).

3.2.2 Size Exclusion Chromatography

Superdex 200 GL column equilibrated with PBS was used to load the *BaPurE* (5 mg/mL) sample. For calibration curve, protein standards were used. Blue dextran (2000 kDa) was the

standard used to measure the void volume of the column. Other standards used were ferritin (440 kDa), β -amylase (200 kDa), aldolase (158 kDa), albumin (66 kDa) and chymotrypsinogen A (25 kDa) (Pharmacia LKB, Piscataway, NJ). Partition coefficient (K_{av}) of each protein standard was calculated using the following equation:

$$K_{av} = \frac{V_e - V_0}{V_t - V_0}$$

where V_0 is the void volume (Blue dextran, 7.3 mL), V_e is the elution volume of a given protein standard and V_t is the total column volume (22.6 mL). Flow rate of 0.5 mL per minute was used at room temperature. The plot of K_{av} vs hydrodynamic molar mass (MW_H) of protein standards was analyzed with linear regression fit, and used as the calibration curve to determine BaPurE's MW_H .

3.2.3 Enzymatic Activity and Ionic Strength

See 2.2.6. Enzymatic activity assay was carried out in 5P7.4- and 25TRIS7.4- with 0 to 150 mM NaCl.

3.2.3.1 CAIR Synthesis

Substrate CAIR was synthesized, following a published protocol (Sullivan *et al.*, 2014), from 5-Amino-1-(β -D-ribofuranosyl)-4-carboxamide-5'-phosphate (AICAR) (Sigma, St. Louis, MO). The synthesis was carried out with Robel Demissie (Fung group). LiOH (1M, 8 mL, Sigma, St. Louis, MO) was added to 50 mg of AICAR in a 10 mL round bottom flask sealed with a septum with a vent at 125 °C under N_2 gas for a total of 4 hours (with complete seal without vent for the last 2 hours). Deionized water (2 mL) was added to the reaction mixture cooled to

room temperature with stirring. pH of the mixture was adjusted 2 N hydrochloric acid to 7 at 0 °C using pH test strips (Sigma, St. Louis, MO) to monitor the pH values. Particulate was removed from the mixture with a cotton/sand column by forced air pressure using a syringe, and the filtrate was lyophilized, yielding white powder. Resulting solid was further purified by resuspension in cold absolute ethanol (15 mL per wash, 3 washes) and by being forced through a cotton/sand column by air pressure. CAIR remaining in the column was recovered by washing with cold deionized water (20 mL) and lyophilized, yielding white powder. CAIR was prepared to a concentration of 1.8 mM in 25TRIS7.4-0 buffer and was stored at -80 °C in 50 µL aliquots for single usage in enzyme activity assay.

Extinction coefficient was calculated using the Beer's law: $\text{Absorbance} = \epsilon L c$ where ϵ is the molar extinction coefficient, L is the pathlength (1 mm) and c is the concentration of the CAIR sample.

3.2.3.2 Samples in Buffers with Different Ionic Strength

Buffers were prepared as 5 mM phosphate pH 7.4 with 0 to 150 mM NaCl and 25 mM TRIS pH 7.4 with 0 to 150 mM NaCl. Ionic strength of a given buffer was determined at room temperature (23 - 25 °C) with a conductivity probe (YSI 3417).

To prepare *BaPurE* samples in different ionic strength buffers, previously prepared *BaPurE* stored in PBS was thawed, centrifuged (Sorvall Legend RT at 3400sg for 2 min) for dialysis. *BaPurE* sample (around 1 mg/ml concentration) were dialyzed at 4 °C in buffers (1:500 protein to buffer ratio) of varying ionic strength for equilibration for 16 to 20 hours using a dialysis tubing (140 kD). Dialyzed samples of *BaPurE* were diluted further in matching buffer to be used for enzymatic assay.

3.2.4 Circular Dichroism

Ellipticity of *BaPurE* samples in buffers of varying conductivity was monitored using a circular dichroism spectrometer (J-810, Jasco, Oklahoma City, OK) with a temperature control unit (PTC-423S) at 25 °C.

3.2.4.1 Secondary Structure

Ellipticity of *BaPurE* (44 to 61 µM, 200 µL) was measured from 200 to 250 nm in a 0.1 mm path length cuvette at 25 °C. Measured Ellipticity (mdeg) was converted to mean residue ellipticity ($[\theta]_{MRW, \lambda}$) by the equation:

$$[\theta]_{MRW, \lambda} = \frac{100 \cdot \theta_{obs, \lambda}}{C_{MR} \cdot d} \text{ deg cm}^2 \text{ dmol}^{-1}$$

where $\theta_{obs, \lambda}$ is the observed ellipticity in degrees, C_{MR} is protein's molar concentration multiplied by the number of amino acids in the protein, d is the cuvette path length (cm) and c is protein concentration in (g/mL). CD spectrum of *BaPurE* in 5 mM phosphate and 25 mM TRIS buffer with pH of 7.4 with 0 to 150 mM NaCl was measured.

3.2.4.2 Tertiary Structure

BaPurE (87 to 150 µM, 1 mL) was measured from 250 to 320 nm in a 1 cm path length cuvette at 25 °C. Signals from single tryptophan (15W), four tyrosine and two phenylalanine per monomer of *BaPurE* (there are no cysteine residues) was detected in the near-UV region. The ellipticity was normalized for concentration (not for residue) with unit mdeg·cm²/M.

3.2.5 Fluorescence

Single tryptophan residue per monomer of *BaPurE* (10 µM, 100 µL) was monitored for

fluorescence by spectrofluorimeter (Jasco FP6200) with temperature control unit (ETC-272T) and cooling unit (Julabo AWC100) in 1 mm path length cuvette. Fluorescence spectra of *BaPurE* was measured under various buffer conditions ($\lambda_{\text{EX}} = 295 \text{ nm}$, $\lambda_{\text{EM}} \sim 350 \text{ nm}$).

3.2.5.1 Tryptophan Quenching with Acrylamide

L-tryptophan solution was prepared in PBS and was titrated with 10 M acrylamide prepared in deionized water. The volume of the L-tryptophan sample was 100 μL in a 1 mm path length cuvette and was titrated with acrylamide. The final volume was 105 μL with final acrylamide concentration of 0.5 M. *BaPurE* (10 μM) was titrated in the same manner as with L-tryptophan with acrylamide. λ_{max} of emission was determined for a given sample to monitor the change in fluorescent intensity upon addition of acrylamide. Fluorescent intensity was adjusted for concentration of L-tryptophan.

Modified Stern-Volmer equation was used to determine the K_{sv} for L-tryptophan:

$$F_0 / F = (1 + K_{\text{sv}}[Q])e^{V[Q]}$$

where V is the static quenching constant and value of 0.75 was used corresponding to a sphere of action of 6.7 \AA (Tallmadge *et al.*, 1989).

3.3 Results

3.3.1 Enzymatic Activity Dependence on Ionic Strength

3.3.1.1 Buffer conductivity

For 5 mM phosphate buffers with pH 7.4, conductivity ranged from 650 to 13000 μMHO for 0 to 150 mM NaCl. 25 mM TRIS buffers' conductivity ranged from 1650 to 13000 μMHO for 0 to 150 mM NaCl. 5 mM TRIS with 0 mM NaCl (5TRIS7.4-0) was prepared with conductivity

of 450 μMHO . See Table 3.1 for buffer abbreviations and conductivity values for each buffer condition.

Table 3.1. Buffer abbreviations and conductivity

Abbreviation	Buffer type	Concentration (mM)	[NaCl] mM	Conductivity (μMHO)	pH
5P7.4-0	Phosphate	5	0	640	7.4
5P7.4-38	Phosphate	5	38	3900	7.4
5P7.4-50	Phosphate	5	50	5800	7.4
5P7.4-75	Phosphate	5	75	7000	7.4
5P7.4-150	Phosphate	5	150	13000	7.4
5TRIS7.4-0	TRIS	5	0	450	7.4
25TRIS7.4-0	TRIS	25	0	1650	7.4
25TRIS7.4-38	TRIS	25	38	4900	7.4
25TRIS7.4-50	TRIS	25	50	5800	7.4
25TRIS7.4-75	TRIS	25	75	7800	7.4
25TRIS7.4-150	TRIS	25	150	13000	7.4

3.3.1.2 CAIR

6.2 mg CAIR was obtained (30 % yield). ^1H NMR (400 MHz, D_2O 4.67): δ 7.38 (s, 1H), 5.53 (s, 1H), 5.51 (s, 1H), 4.68 - 4.65 (m, 1H). Signal due to decomposition product of CAIR was not observed at 6.4 ppm. Extinction coefficient of synthesized CAIR was $11681 \text{ M}^{-1} \text{ cm}^{-1}$. Extinction coefficient of CAIR was previously reported as $10500 \text{ M}^{-1} \text{ cm}^{-1}$, in literature (Constantine *et al.*, 2006).

3.3.1.3 Enzymatic Activity Dependence on Ionic Strength

BaPurE sample used was prepared with higher yield and purity than that used in HTS studies with new plasmid transformation and adjustment of purification method. Prepared protein was found to be octameric in PBS as shown by the hydrodynamic molecular weight in PBS.

BaPurE appeared to be well folded as seen by secondary structure elements in its CD spectrum.

BaPurE activity showed dependence on buffer ionic strength as shown in Figure 3.1. *BaPurE* is most active in buffer with conductivity from 4000 - 8000 μMHO . The maximum specific activity was 19.2 ± 1.6 units/mg in 5P7.4-75, and specific activity of 6.5 ± 0.7 units/mg in conductivity range below 1000 μMHO (5P7.4-0).

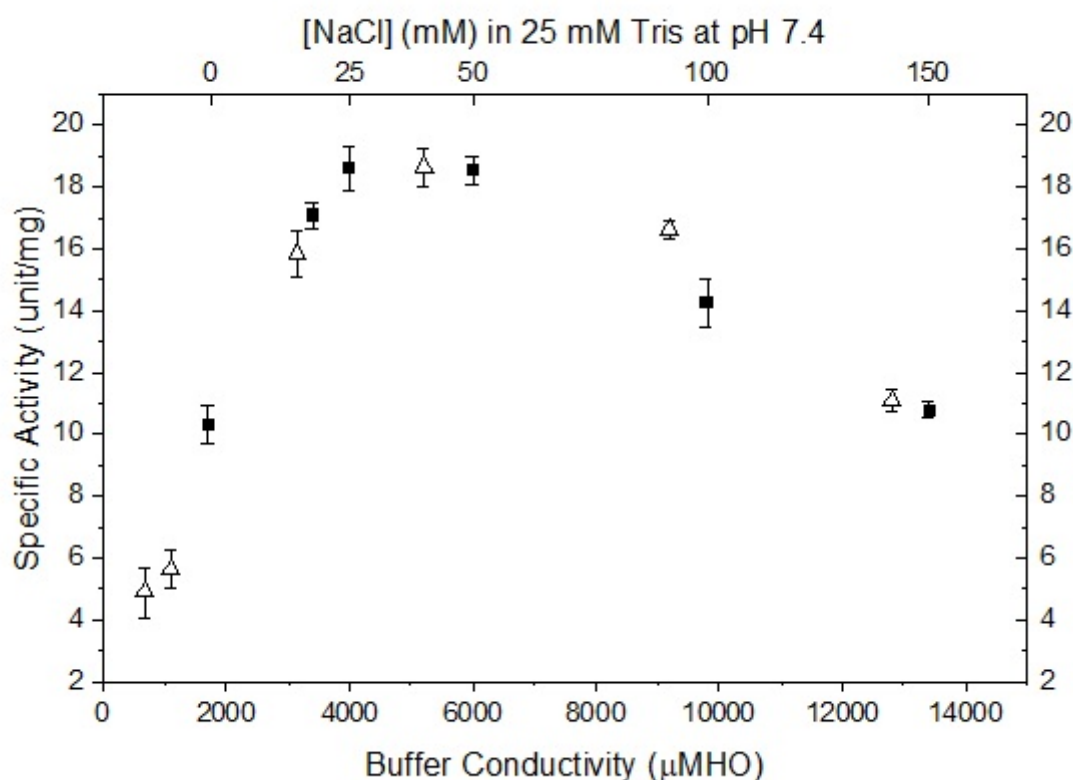


Figure 3.1. Specific activity of *BaPurE* in 25 mM TRIS (filled square) and in 5 mM Phosphate buffer (empty triangle) buffer with 0 - 150 mM NaCl. (Figure originate by Nina M. Wolf; data of Anna K. Jones included).

3.3.2 Secondary and Tertiary Structural Elements

Difference in the amount of secondary structural elements was observed high ionic strength (150 mM NaCl) and low ionic strength (0 mM NaCl), regardless of the type of buffer (Phosphate or TRIS). $[\theta]_{\text{MRW},\lambda}$ amplitude of *BaPurE* was 11% less in low ionic strength than in high ionic strength buffer (Figure 3.2).

Tertiary structure element of *BaPurE* was observed by CD spectra obtained from 250 - 320 nm at 25 °C. The free L-tryptophan, which unstructured, showed very weak CD signal as compared to tryptophan residue in the *BaPurE* monomer complex that showed characteristic tryptophan peak at 291 nm with negative intensity (Figure 3.3). There was 20% reduction in ellipticity resulting from tryptophan residue at 291 nm in low ionic strength buffer when compared with that in high ionic strength buffer.

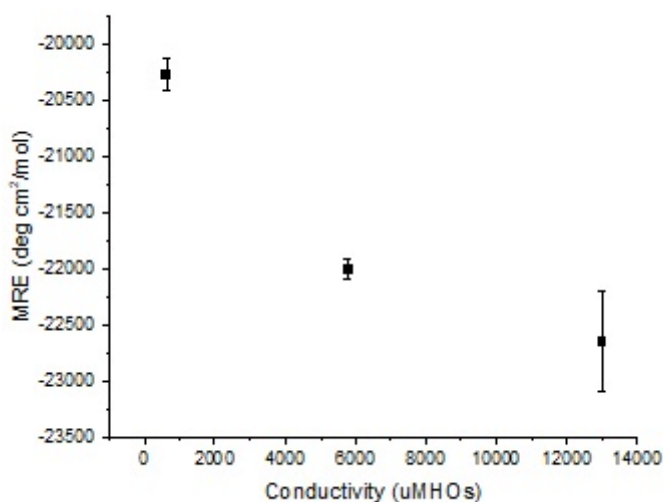


Figure 3.2. Mean residue ellipticity of *BaPurE* in low to high ionic strength buffer (n = 7).

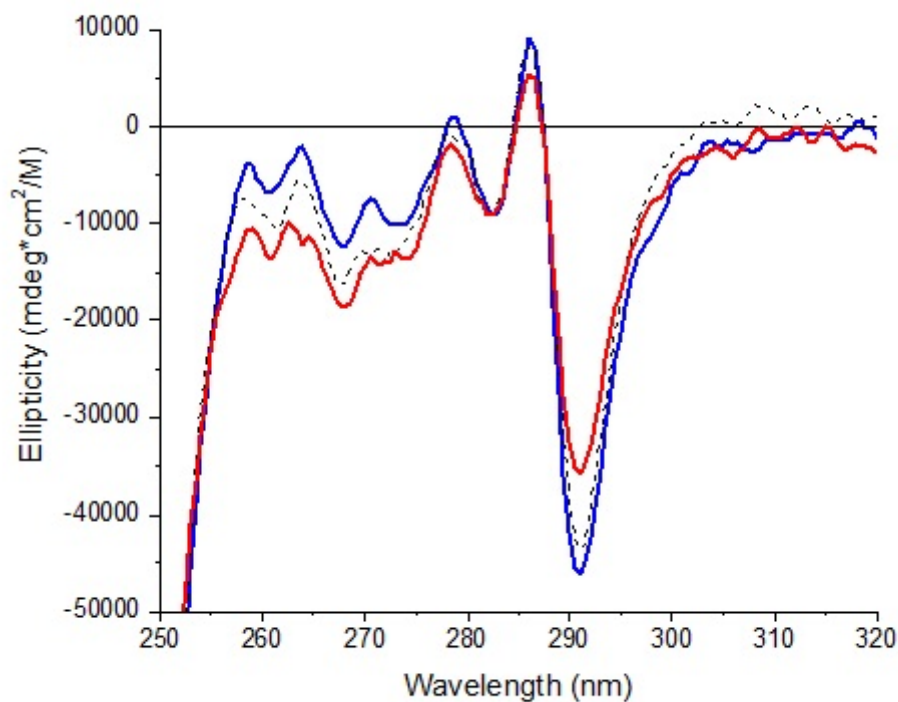


Figure 3.3. Near UV-CD spectrum of *BaPurE* in high ionic strength (13000 μMHO , blue, solid), medium ionic strength (5800 μMHO , black, dotted), low ionic strength (640 μMHO , red, solid), and L-tryptophan in PBS (black, solid).

3.3.3 Tryptophan Accessibility

K_{SV} of free L-tryptophan quenching was $20.9 \pm 0.6 \text{ M}^{-1}$ ($n = 3$). K_{SV} of completely unfolded *BaPurE* in presence of 9 M urea in 5P7.4-150 buffer was 10.2 M^{-1} .

Highest K_{SV} of native *BaPurE* was $4.9 \pm 0.5 \text{ M}^{-1}$ ($n = 3$) in 5TRIS7.4-0 buffer with conductivity of 450 μMHO (very low ionic strength). In low to high ionic strength (1000 - 13000 μMHO) buffer, K_{SV} of *BaPurE* was around 2.0 M^{-1} .

3.4 Discussion

Understanding of *BaPurE* solution property including its stability and conformation state with correlation to enzyme activity can provide useful information for further studies in antibacterial lead identification for this essential enzyme in *de novo* purine biosynthesis pathway.

The specific activity of *BaPurE* showed its most active state in medium ionic strength buffer with conductivity between 5000 to 8000 μMHO , and its least active state in buffers with conductivity below 1000 μMHO which was correlated with different conformational states of *BaPurE*. From this finding, it can be assumed that various conformational states of *BaPurE* consist of less active to more active state.

To investigate *BaPurE* structure that causes it to be more or less active, secondary structure of *BaPurE* in low to high ionic strength buffer was examined. Difference between the low to high ionic strength buffer showed 11% difference in the amount of α -helix present where more α -helix was found in high ionic strength buffer. This suggests that *BaPurE* is in a less folded conformation in low ionic strength than in higher ionic strength buffer. Signal from 15W residue of tertiary structure was decreased by 20% in low ionic strength buffer compared to medium to high ionic strength buffer which suggests looser structure in low ionic strength condition as seen by the absence of tertiary signal of free L-tryptophan.

Accessibility of tryptophan residue in *BaPurE* was assessed with neutral quencher molecule acrylamide. K_{sv} of free L-tryptophan agreed with published value of $21 \pm 3 \text{ M}^{-1}$ (Tallmadge *et al.*, 1989). Equation used to calculate K_{sv} corrects for the static quenching component to describe both static and dynamic quenching mode free-L-tryptophan undergoes (Tallmadge *et al.*, 1989). There was not much difference in K_{sv} between 5000 to 13000 μMHO

conductivity. The subtle conformational differences between buffers of medium to high ionic strength is not revealed by difference in tryptophan accessibility. This is expected since the crystal structure of *BaPurE* shows the tryptophan residue to be on the well exposed part of the enzyme whose environment will not be very different with slight conformational differences. There is a detectable difference in K_{sv} in very low (less than 1000 μ MHO) ionic strength conditions. K_{sv} of very low ionic strength buffer is about 2 times greater, suggesting that *BaPurE* is in a more unfolded conformation.

Identification of inhibitors of *BaPurE* requires information regarding protein stability as well as conformation in solution. The findings from this study suggest that *BaPurE* is in a well folded state between 4000 to 13000 μ MHO and the most active state is between 4000 - 8000 μ MHO range.

3.5 Conclusion

BaPurE in buffers of different ionic strength provided much insight regarding the behavior and conformational differences. *BaPurE* is most active in medium ionic strength showing correlation of enzyme activity with conformation as a function of ionic strength. Enzymatic activity studies can be carried out with consideration of various conformational states of *BaPurE* in a range of ionic strength. Therefore, activity of *BaPurE* can be further studied in most active condition to determine inhibition activity of a given compound with potential inhibition property.

CHAPTER 4

CHEMICAL UNFOLDING OF *BaPurE*

4.1 Introduction

Proteins in the body undergo folding process to acquire a native conformation to function. The folding process is driven by weak interactions, including hydrophobic effect, and sometimes is assisted by chaperones. When proteins fail to fold into its native conformation, their denatured states often aggregate and accumulate, as in cells of several neuro-degenerative diseases (Selkoe, 2003). Protein folding is an important process and can also be studied through the protein unfolding process. Protein conformational stability can be estimated by the difference in stability of the native and the denatured states, assuming the unfolding reaction is reversible (Pace, 1986).

Unfolding of a protein can be carried out by adding chemical denaturant such as urea and Gdn-HCl, gradually to maintain equilibrium at all steps to give a reversible folding and unfolding process. Equilibrium unfolding can be used to determine the conformational stability of proteins. With a two states assumption, the folded (N) and unfolded (D) states of a protein are in equilibrium ($N \rightleftharpoons D$) in solution. To measure the protein stability, the equilibrium can be shifted toward the unfolded state by gradually adding chemical denaturant to a protein solution. The equilibrium constant of unfolding at each denaturant concentration (K_D) is related to the free energy change since $K_D = \exp(-\Delta G_D/RT) = f_U/f_N$, where f_U was the fraction of unfolded protein with denaturant concentration of [D] and f_N was the fraction of remaining folded protein. ΔG_D at each denaturant concentration can be used to estimate the conformational stability. In the linear extrapolation model (Meyer *et al.*, 1995), $\Delta G_D = \Delta G^{H_2O} - m [\text{denaturant}]$, where ΔG^{H_2O} ,

representing conformational stability, is extrapolated from the plot of experimental values of ΔG_D at different [D] to a value where [D] = 0. The slope of the plot, m , has a strong correlation between the accessible surface area exposed upon unfolding, or the difference in the accessible surface area between the unfolded and folded state of the protein (Pace, 1986).

Proteins bind denaturant molecules to expose peptide groups (Courtenay *et al.*, 2000). Due to the differences in the ionic charge of urea and Gdn-HCl molecules, differential binding of the denaturant molecules to proteins has been extensively studied (Pace, 1986). Urea is known to promote protein unfolding directly (formation of intramolecular hydrogen bond) and indirectly (alteration of water structure surrounding the protein molecule to promote hydrophobic solvation) (Bennion and Daggett, 2003). Gdn-HCl ions mask electrostatic interactions in proteins, revealing the importance of electrostatic interactions in protein folding (Monera *et al.*, 1994). Due to these differences, urea and Gdn-HCl denaturations provide different estimates of stability for proteins.

In this chapter, I discuss the chemical unfolding of *BaPurE* by urea and by Gdn-HCl in buffers with different ionic strength conditions to obtain information on the protein stability.

4.2 Experimental Procedures

4.2.1 Protein Preparation

See section 2.3.1 for *BaPurE* purification, and *BaPurE* in buffers (5 mM phosphate or 25 mM TRIS at pH 7.4) of different ionic strengths was used. NaCl at different concentrations (0 - 150 mM) was added to either the phosphate or the TRIS buffer to give low (1,650 μ MHO), medium (5,800 μ MHO) or high (13,000 μ MHO) buffer solutions. See section 3.3.1.1 for details.

4.2.2 Chemical Unfolding of *BaPurE* by Circular Dichroism Method

Chemical denaturant stock solutions, Gdn-HCl (8 M) and urea (10 M), were prepared in

buffers matching the buffer condition of *BaPurE* samples. The conductivity was lowered when urea was added, but was increased when Gdn-HCl was added, to a given buffer. For example, the buffer with conductivity of 13,000 μMHO was lowered to 8,100 μM when 8 M urea was added, but was increased to 80,000 μMHO when 7M Gdn-HCl was added.

Gdn-HCl or urea stock solution was added in aliquots to *BaPurE* sample to prepare a series of *BaPurE* samples with different concentrations of Gdn-HCl or urea. Final protein concentration in each sample with denaturant added was calculated according to the dilution factor. A circular dichroism spectrometer (Jasco Model J-810, Oklahoma City, OK) with a temperature control unit (PTC-423S) was used to obtain CD spectrum, between 200 to 250 nm, of each protein sample with a specific urea or Gdn-HCl concentration, [D]. The raw ellipticity value (mdeg) at 222 nm was extracted from the CD spectrum and converted to molar residue ellipticity (MRE, θ , $\text{deg cm}^2/\text{dmol}$), with $\theta = ((\text{raw ellipticity}) * 100) / (0.1 * 164 * [\text{BaPurE}] (\mu\text{moles/mL}))$ (Figure 4.1 A). The θ value of a sample with a specific [D] was θ_D . $\theta_N = \theta_D$ when [D] = 0 where θ_N is θ value of a sample with [D] = 0, and $\theta_U = \theta_D$ when [D] = [D]_{max}, a concentration at which the CD signal of θ_U (θ value of fully unfolded sample) was no longer changing upon further additional of urea or Gdn-HCl. [D]_{max} = 8 M for urea, and 7 M for Gdn-HCl.

The unfolding fraction of *BaPurE* at a particular [D], $f_U(D)$, was obtained from the θ values since $f_U(D) = (\theta_D - \theta_N) / (\theta_U - \theta_N)$. The denaturation profile, the plot of $f_U(D)$ versus [D], was fitted by a Boltzmann function, provided by a software (OriginPro, 2016), $f_U(D) = (A_1 - A_2) / (1 + \exp([D] - [D_{50}]))$, where $A_1 = f_U([D] = 0) = 0$, $A_2 = f_U([D] = [D]_{\text{max}}) = 1$ and [D]₅₀ was the concentration of urea or Gdn-HCl where $f_U(D) = 0.5$, the 50% threshold (Figure 4.1.A). In our analysis, only the values of $f_U(D)$ between 0.1 and 0.9, rather than 0 to 1,

were used. The free energy change, ΔG_D , was from the equilibrium concentration ($K_D = \exp(-\Delta G_D/RT) = f_U/f_N$), and the ΔG^{H_2O} and m values were obtained from the plot of ΔG_D versus $[D]$ (Figure 4.1.B). The slope of the plot was m -value, and the ΔG^{H_2O} was ΔG_D when $[D] = 0$.

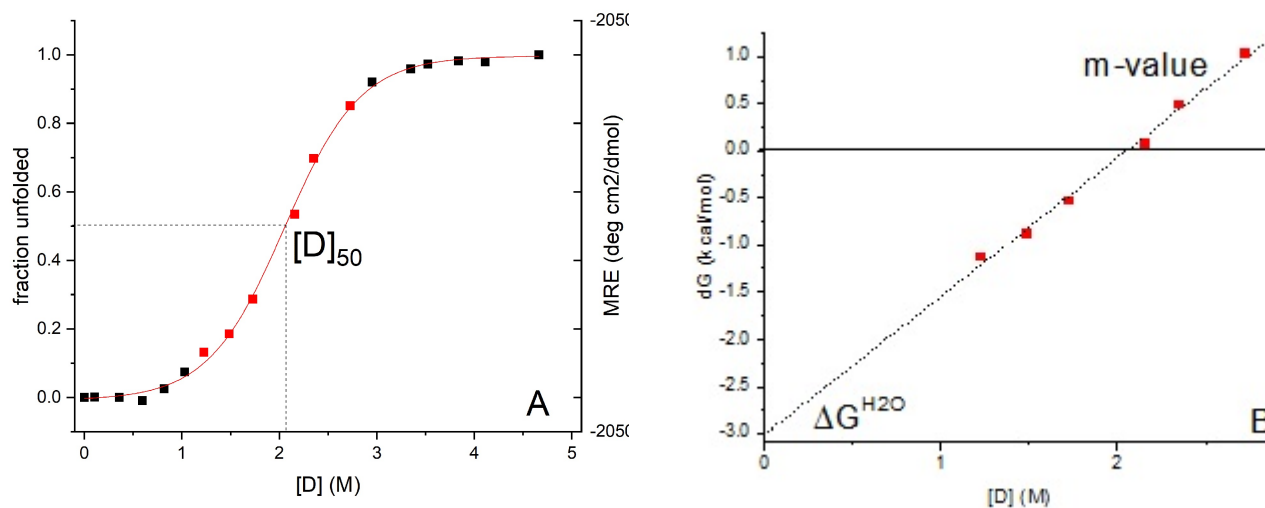


Figure 4.1. A. Equilibrium denaturation curve where shift of unfolded *BaPurE* is observed upon denaturant concentration. The CD measurements of raw ellipticity were converted to molar residue ellipticity (MRE, θ , deg cm²/dmol) (right-hand-side y axis). The corresponding unfolded fractions of *BaPurE* (left-hand-side y axis), with values between 0.1 to 0.9 are in red and were used for curve fitting, while the unfolded fractions of *BaPurE* not used for curve fitting are in black. B. ΔG_D plotted with denaturant concentration with linear fit to give m -value (slope, dotted line) and ΔG^{H_2O} as y-intercept ($[D] = 0$).

4.3 Results

4.3.1 Chemical Unfolding of *BaPurE* in Guanidium Chloride

4.3.1.1 Effect of different ionic strength buffer on unfolding

The plots of the results from a typical run of all three ionic strength conditions, fraction unfolded versus [Gdn-HCl], is shown in Figure 4.2.A. The average [Gdn-HCl]₅₀ required to unfold 50% of *BaPurE* was 2.2 ± 0.04 M (n = 6) in low ionic strength buffer, 2.5 ± 0.11 M (n = 4) in medium ionic strength buffer and to 2.7 ± 0.03 M (n = 5) in high ionic strength buffer A summary of these values are shown in Table 1.

A typical plot of [Gdn-HCl] versus ΔG_D of Gdn-HCl for all three ionic strength conditions is shown in Figure 4.2.B. The average m-value from Gdn-HCl denaturation was 1.8 ± 0.16 kcal/mol M (n = 6) in low ionic strength buffer, 2.0 ± 0.18 kcal/mol M (n = 4) in medium ionic strength buffer and 1.8 ± 0.20 kcal/mol M in high ionic strength buffer (Table 4.1). ΔG^{H_2O} obtained from the above results was -3.8 ± 0.37 kcal/mol (n = 6) in low ionic strength buffer, -5.1 ± 0.66 kcal/mol (n = 4) in medium ionic strength buffer and -4.9 ± 0.49 kcal/mol (n = 5) in high ionic strength buffer (Table 4.1).

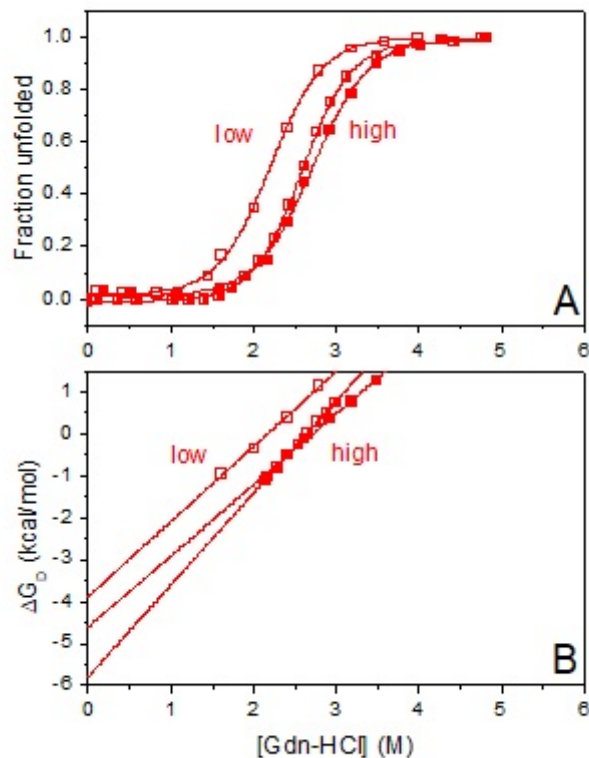


Figure 4.2. A. The results of a typical run on the fraction unfolded versus [Gdn-HCl] in buffers with three ionic strength conditions, in 1650 μ MHO (low, empty square), in 5800 μ MHO (medium, half-filled square), and in 13000 μ MHO (high, filled square). The $[\text{Gdn-HCl}]_{50}^{\text{low}} = 2.20$ M, $[\text{Gdn-HCl}]_{50}^{\text{medium}} = 2.59$ M, $[\text{Gdn-HCl}]_{50}^{\text{high}} = 2.71$ M. The average values of $[\text{Gdn-HCl}]_{50}$ are shown in Table 1.

B. ΔG_D of *BaPurE* versus [Gdn-HCl] in buffers with three ionic strength conditions, with an $m\text{-value}^{\text{low}} = 1.79$ kcal/mol M and $\Delta G^{\text{H}_2\text{O}, \text{low}} = -3.87$ kcal/mol for low ionic strength buffer, $m\text{-value}^{\text{medium}} = 2.19$ kcal/mol M and $\Delta G^{\text{H}_2\text{O}, \text{medium}} = -4.60$ kcal/mol in medium ionic strength buffer, and $m\text{-value}^{\text{high}} = 1.69$ kcal/mol M and $\Delta G^{\text{H}_2\text{O}, \text{high}} = -4.60$ kcal/mol in high ionic strength buffer. The average values are shown in Table 1.

4.3.2 Chemical Unfolding of *BaPurE* in Urea

4.3.2.1 Effect of different ionic strength buffer on unfolding

The plots of the results from a typical run of all three ionic strength conditions, fraction unfolded versus [urea], is shown in Figure 4.3.A. The average [urea]₅₀ required to unfold 50% of *BaPurE* was 1.7 ± 0.01 (n = 3) in low ionic strength buffer, 2.8 ± 0.20 M (n = 4) in medium ionic strength buffer and 4.3 ± 0.07 M (n = 7) in high ionic strength buffer (Table 4.1). Also shown in Table 4.1 are the ratios of [Gdn-HCl]₅₀ to [urea]₅₀. They were 1.3 for low ionic strength buffer, 0.9 for medium ionic strength buffer and 0.6 for high ionic strength buffer.

A typical plot of [urea] versus ΔG_D of urea for all three ionic strength conditions is shown in Figure 4.3.B. The average m-value from urea denaturation was 1.7 ± 0.13 kcal/mol (n = 3) in low ionic strength buffer, 1.3 ± 0.09 kcal/mol (n = 4) in medium ionic strength buffer and 1.0 ± 0.13 kcal/mol M (n = 7) in high ionic strength buffer (Table 4.1). Also shown in Table 4.1 are the ratios of m-value (Gdn-HCl) to m-value (urea). They were 1.06 for low ionic strength buffer, 1.54 for medium ionic strength buffer and 1.80 for high ionic strength buffer.

ΔG^{H_2O} from urea denaturation results was -2.9 ± 0.24 kcal/mol (n = 3) in low ionic strength buffer, -3.5 ± 0.30 kcal/mol (n = 4) in medium ionic strength buffer and -4.4 ± 0.55 kcal/mol (n = 7) in high ionic strength buffer (Table 4.1).

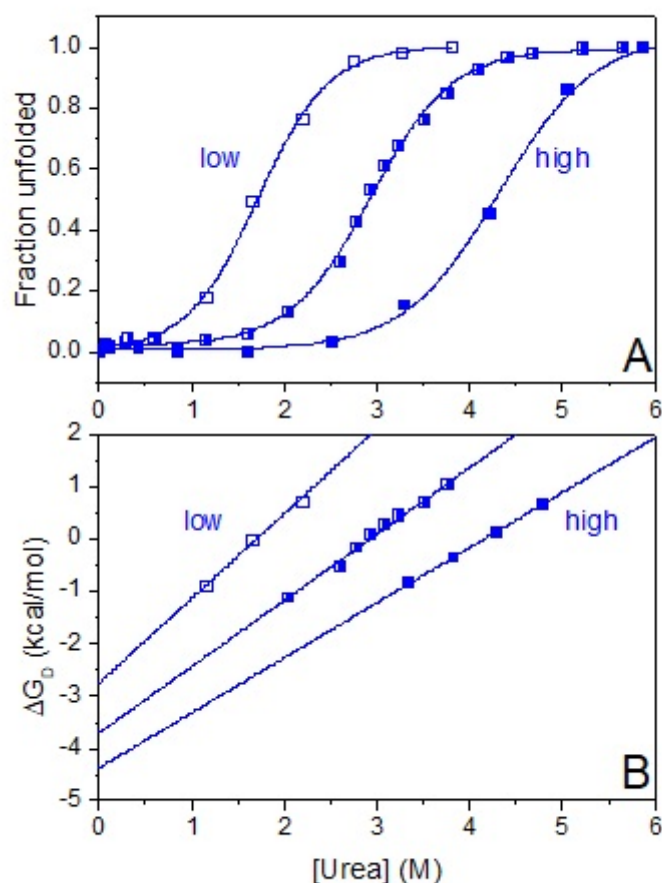


Figure 4.3. A. The results of a typical run on the fraction unfolded versus [urea] in buffers with three ionic strength conditions, in 1650 μ MHO (low, empty square), in 5800 μ MHO (medium, half-filled square), and in 13000 μ MHO (high, filled square). The $[\text{Urea}]_{50}^{\text{low}} = 1.71 \text{ M}$, $[\text{Urea}]_{50}^{\text{medium}} = 2.93 \text{ M}$, $[\text{Urea}]_{50}^{\text{high}} = 4.32 \text{ M}$. The average values of $[\text{urea}]_{50}$ are shown in Table 4.1.

B. ΔG_D of *BaPurE* versus [urea] in buffers with three ionic strength conditions, with an $m\text{-value}^{\text{low}} = 1.54 \text{ kcal/mol M}$ and $\Delta G^{\text{H}_2\text{O}, \text{low}} = -2.67 \text{ kcal/mol}$ for low ionic strength buffer, $m\text{-value}^{\text{medium}} = 1.27 \text{ kcal/mol M}$ and $\Delta G^{\text{H}_2\text{O}, \text{medium}} = -3.71 \text{ kcal/mol}$ for medium ionic strength buffer, and $m\text{-value}^{\text{high}} = 1.04 \text{ kcal/mol M}$ and $\Delta G^{\text{H}_2\text{O}, \text{high}} = -4.71 \text{ kcal/mol}$ for high ionic strength buffer.

value^{high} = 1.05 kcal/mol M and $\Delta G^{\text{H}_2\text{O, high}}$ = -4.38 kcal/mol for high ionic strength buffer. The average values are shown in Table 4.1.

Table 4.1. The average (Avg) and standard deviation (SD) values of the denaturation of *BaPurE* by Gdn-HCl and by urea in buffers with low ionic strength, medium ionic strength and high ionic strength conditions. Circular dichroism spectroscopy methods were used to follow the denaturation in each sample.

Conductivity ^a (μMHO)	[D] ₅₀ (M) ^b				[G] ₅₀ /[Urea] ₅₀ ^c	m-value (kcal mol ⁻¹ M ⁻¹) ^d				m ^{Gdn-HCl} /m ^{urea} ^e	ΔG ^{H₂O} (kcal mol ⁻¹) ^d			
	Gdn-HCl		Urea			Gdn-HCl		Urea			Gdn-HCl		Urea	
	Avg	SD	Avg	SD		Avg	SD	Avg	SD		Avg	SD	Avg	SD
1650	2.2	0.04 (<i>n</i> = 6)	1.7	0.01 (<i>n</i> = 3)	1.3	1.8	0.16 (<i>n</i> = 6)	1.7	0.13 (<i>n</i> = 3)	1.06	-3.8	0.4 (<i>n</i> = 6)	-2.9	0.24 (<i>n</i> = 3)
5800	2.5	0.1 (<i>n</i> = 4)	2.8	0.20 (<i>n</i> = 4)	0.9	2.0	0.18 (<i>n</i> = 4)	1.3	0.09 (<i>n</i> = 4)	1.54	-5.1	0.7 (<i>n</i> = 4)	-3.5	0.30 (<i>n</i> = 4)
13000	2.7	0.03 (<i>n</i> = 5)	4.3	0.07 (<i>n</i> = 7)	0.6	1.8	0.16 (<i>n</i> = 6)	1.0	0.13 (<i>n</i> = 7)	1.80	-4.9	0.5 (<i>n</i> = 6)	-4.4	0.55 (<i>n</i> = 7)

^aThe conductivity values were of 5 mM phosphate buffer with NaCl before adding Gdn-HCl or urea. The conductivity value was lowered when urea was added, but was increased when Gdn-HCl was added, to a given buffer. For example, the buffer with conductivity of 13,000 μ MHO was lowered to 8,100 μ M when 8 M urea was added, and was increased to 80,000 μ MHO when 7M Gdn-HCl was added.

^b [D]₅₀ represent concentration of Gdn-HCl or urea required to unfold 50% of *BaPurE*. The average and standard deviation values are given.

^c [Gdn-HCl]₅₀ / [Urea]₅₀.

^d Determined from free energy vs denaturant concentration plot.

^e m-value^{Gdn-HCl}/m-value^{urea}

4.4 Discussion

As discussed in literature, with all equilibrium techniques for monitoring protein denaturation as a function of solvent composition, the primary data consist of a sigmoidal curve representing a change in physical parameter (Shortle and Meeker, 1986). *BaPurE* in the presence of either Gdn-HCl or urea exhibited similar sigmoidal curves. The characteristic parameters ($[D]_{50}$, m -values and ΔG^{H_2O}) obtained from equilibrium unfolding of *BaPurE* by charged Gdn-HCl or by neutral urea were generally consistent with published values of other protein (*e.g.*, Pradeep and Udgaonkar, 2004; Myer, 1995; Pace *et al.*, 1987; Shortle and Meeker, 1986; Greene and Pace, 1974).

The $[Gdn-HCl]_{50}$ values increased slightly (from 2.2 to 2.7 M) despite the large increase in ionic strength, with the *BaPurE* sample buffer conductivity increased from 1650 to 13000 μ MHO. The actual conductivity values in each sample with Gdn-HCl were higher since the addition of Gdn-HCl increased the conductivity (the value was 80,000 μ MHO when 7M Gdn-HCl was added to the buffer of 13,000 μ MHO). It was demonstrated that the ionic nature of Gdn-HCl mask electrostatic interactions in model protein of 4 coiled-coil analogue where similar $[Gdn-HCl]_{50}$ values (3.5 to 3.6 M for all attractive forces and all repulsive forces respectively) were observed regardless of how many intra- or interchain electrostatic attractions or repulsions were present (Monera *et al.*, 1994).

The $[urea]_{50}$ values increased significantly (from 1.7 to 4.3 M) upon increasing solution ionic strength. The actual conductivity values in each sample with urea were lower since the addition of urea decreased the conductivity (the value was 8,100 μ MHO when 8 M urea was added to the buffer of 13,000 μ MHO), suggesting that *BaPurE* was more stable under high ionic

strength condition. The m-values decreased slightly, from 1.7 to 1.0, upon changing the ionic strength, from low salt buffer to high salt (150 mM NaCl) buffer. The m-value correlates strongly with the amount of protein surface exposed to solvent upon unfolding (Myers *et al.*, 1995). Thus the m-values for *BaPurE* suggested that the amount of protein surface exposed to solvent in its native form, without denaturant, was higher in low-salt buffers than high-salt buffers.

It has been suggested that the solubilizing ability of Gdn-HCl relative to urea is greater for polar groups than for nonpolar groups (Greene and Pace, 1974). Thus, our results that *BaPurE* consisted of more nonpolar groups than polar groups in the interior. This is validated by its crystal structure (PDB code:1XMP).

The $\Delta G^{\text{H}_2\text{O}}$ values obtained from both Gdn-HCl and urea studies were higher for high salt conditions (from 3.8 to 4.9 kcal mol⁻¹ for Gdn-HCl and from 2.9 to 4.4 kcal mol⁻¹ for urea studies) also suggest that *BaPurE* was more stable in high-salt than low-salt conditions.

4.5 Conclusion

The study of differences between Gdn-HCl and urea gave molecular level understanding of electrostatic interactions of *BaPurE*. In different ionic strength conditions, the degree of overall attractive interaction between residues and surface electrostatic interaction was variable. *BaPurE* assumes a more compact conformation in high ionic strength conditions due to higher attractive interactions while having low surface interaction between charged groups. Ionic strength induced conformations of *BaPurE* should be taken into consideration when searching for inhibitors that bind to *BaPurE*.

REFERENCES

Aminov, I. Rustam. (2010) A brief history of the antibiotic era: lessons learned and challenges for the future. *Frontiers in Microbiology* 1: 134.

Anderson, A. (2003) The process of structure-based drug design. *Chemical Biology* 10: 787 - 797.

Ball P., Baquero F., Cars O., File T., Garau J., Klugman K., Low D.E., Rubinstein E., and Wise R. (2002) Antibiotic therapy of community respiratory tract infections: strategies for optimal outcomes and minimized resistance emergence. *Journal of Antimicrobial Chemotherapy* 49: 31-40.

Barker J. J. (2006) Antibacterial drug discovery and structure-based design. *Drug Discovery Today* 11: 391-404.

Bennion B. J. and Daggett V. (2003) The molecular basis for the chemical denaturation of proteins by urea. *Proceedings of the National Academy of Sciences* 100: 5142-5147.

Bergman N. H., Anderson E. C., Swenson E. E., Janes B. K., Fisher N., Niemeyer M. M., Miyoshi A. D., and Hanna P. C. (2007) Transcriptional Profiling of *Bacillus anthracis* during Infection of Host Macrophages. *Infection and Immunity* 75: 3434–3444.

Boyle M. P., Kalliomaa A. K., Levnikov V., Blagova E., Fogg M. J., Brannigan J. A., Wilson K.S., and Wilkinson A. J. (2005) Crystal Structure of PurE (BA0288) from *Bacillus anthracis* at 1.8 Å Resolution. *Proteins: Structure, Function, and Bioinformatics* 61: 674–676.

Brook I., Elliott T. B., Pryor II H. I., Sautter T. E., Gnade, Jayendrakumar B. T., Thakar H., and Knudson G. B. (2001) In vitro resistance of *Bacillus anthracis* Sterne to doxycycline, macrolides and quinolones. *International Journal of Antimicrobial Agents* 18: 559–562.

Bull H. B. and Breese K. (1965) Ionization of ribonuclease. *Archives of Biochemistry and Biophysics* 110: 331-336.

Chan C. Y., Zhaob H., Pugh R. J., Pedley A. M., French J., Jones S. A., Zhuang X., Jinna H., Huang T. J., and Benkovic S. J. (2015) Purinosome formation as a function of the cell cycle. *Proceedings of the National Academy of Sciences* 112: 1368-1373.

Chang, J. Y., Alkan, S. S., Hilschmann, N., and Braun, D. G. (1985) Thrombin specificity. Selective cleavage of antibody light chains at the joints of variable with joining regions and joining with constant regions. *Federation of European Biochemical Societies* 151: 225-230.

Christodoulou, E. and Vorgias, C. E. (2002) Understanding heterologous protein overproduction under the T7 promoter. *Biochemistry and Molecular Biology Education* 30: 189 - 191.

Constantine C. Z., Starks C. M., Mill C. P., Ransome A. E., Karpowicz S. J., Francois J. A., Goodman R. A., and Kappock T. J. (2006) Biochemical and structural studies of N5-carboxyaminoimidazole ribonucleotide mutase from the acidophilic bacterium acetobacter aceti. *Biochemistry* 45: 8193-8208.

Courtenay E. S., Capp M. W., Saeker R. M., and Record M. T. Jr. (2000) Thermodynamic analysis of interactions between denaturants and protein surface exposed on unfolding: Interpretation of urea and guanidinium chloride m-values and their correlation with changes in accessible surface area (ASA) using preferential interaction coefficients and the local-bulk domain model. *Proteins Structure Function Bioinformatics* 41: 72-85.

Farkas V., Jakli I., Toth G. K., and Perczel A. (2016) Aromatic cluster sensor of protein folding: Near-UV electronic circular dichroism bands assigned to fold compactness. *Chemistry - A European Journal* 22: 13871-13883.

Ferguson A. D., Sheth P. R., Basso A. D., Paliwal S., Gray K., Fischmann T. O., and Le H. V. (2011) Structural basis of CX-4945 binding to human protein kinase CK2. *Federation of European Biochemical Societies Letters* 585: 104–110.

Firestine S. M., Poon S., Mueller E. J., Stubbe J., and Davisson V. J. (1994) Reactions catalyzed by 5-aminoimidazole ribonucleotide carboxylases from *Escherichia coli* and *Gallus gallus*: a case for divergent catalytic mechanisms? *Biochemistry* 33: 11927-11934.

Firestine S. M., Wu W., Youn H., and Davisson V. J. (2009) Interrogating the mechanism of a tight binding inhibitor of AIR carboxylase. *Bioorganic Chemistry* 17: 794–803.

Greene R. F. and Pace C. N. (1974) Urea and guanidine hydrochloride denaturation of ribonuclease, lysozyme, α -chymotrypsin, and β -lactoglobulin. *The Journal of Biological Chemistry* 249: 5388-5303.

Greenfield, N. J. (2006) Using circular dichroism spectra to estimate protein secondary structure. *Nature Protocols* 1: 2876-2890.

Gross M., Furter-Graves E. M., Wallimann T., Eppenberger H. M., and Furter R. (1994) The tryptophan residues of mitochondrial creatine kinase: Roles of Trp-223, Trp-206, and Trp-264 in active-site and quaternary structure formation. *Protein Science* 3: 1058-1068.

Hagihara Y., Aimonio S., Fink A. L., and Goto Y. (1993) Guanidine hydrochloride-induced folding of proteins. *Journal of Molecular Biology* 231: 180-184.

Hammack B., Attfield K., Clayton D., Dec E., Dong A., Sarisky C., and Bowler B. E. (1998) The magnitude of changes in guanidine-hcl unfolding m-values in the protein, iso-1-cytochrome c, depends upon the substructure containing the mutation. *Protein Science* 7: 1789-1795.

Hansen, L. H., Knudsen, S., and Sorensen, S. J. (1998) The effect of the lacY gene on the

induction of IPTG inducible promoters, studied in *Escherichia coli* and *Pseudomonas fluorescens*. *Current Microbiology* 36: 341-347.

Karginov V. A., Robinson T. M., Riemenschneider J., Golding B., Kennedy M., Shiloach J., and Alibek K. (2004) Treatment of anthrax infection with combination of ciprofloxacin and antibodies to protective antigen of *Bacillus anthracis*. *FEMS Immunology and Medical Microbiology* 40: 71-74.

Kelly S. M., Jess T. J., and Price N. C. (2005) How to study proteins by circular dichroism. *Biochimica et Biophysica Acta* 1751: 119-139.

Kelly S. M. and Price N. C. (2000) The use of circular dichroism in the investigation of protein structure and function. *Current Protein and Peptide Science* 1: 349-384.

Kim A., Wolf N. M., Zhu T., Johnson M. E., Deng J., Cook J. L., Fung L. W.-M. (2015) Identification of *Bacillus anthracis* PurE inhibitors with antimicrobial activity. *Bioorganic & Medicinal Chemistry* 23: 1492-1499.

Kranz, J. K. and Schalk-Hihi, C. (2011) Protein thermal shifts to identify low molecular weight fragments. *Methods in Enzymology* 493: 278 - 296.

Kupferschmidt K. (2016) Evolutionary biologists are challenging old dogmas about the way

antibiotics should be used. *Science* 352: 758-761.

Lee B. L., Padula A. M., Kimbrough R. C., Jones S. R., Chaisson R. E., Mills J., and Sande M. A. (1991) Infectious complications with respiratory pathogens despite ciprofloxacin therapy. *The New England Journal of Medicine* 325: 520-521.

Lo, M.-C., Aulabaugh, A., Jin, G., Cowling, R., Bard, J., Malamas, M., and Ellestad, G. (2004) Evaluation of fluorescence-based thermal shift assays for hit identification in drug discovery. *Analytical Biochemistry* 332: 153 - 159.

Macarron, R. and Hertzberg, R. P. (2009) Design and implementation of high throughput screening assays. *Methods in Molecular Biology* 565: 1 - 32.

Missiakas, D. M., and Schneewind, O. Editors: Lindler, L. E., Lebeda, F. J., and Korch, G. W. (2005) *Infectious diseases: biological weapons defense: infectious diseases and counterterrorism*. Humana Press, Totowa, NJ: pp. 79 - 97.

Moller M. and Denicola A. (2002) Protein Tryptophan Accessibility Studied by Fluorescence Quenching. *Biochemistry and Molecular Biology Education* 30: 175-178.

Monera O. D., Kay C. M., and Hodges R. S. (1994) Protein denaturation with guanidine hydrochloride or urea provides a different estimate of stability depending on the contributions of

electrostatic interactions. *Protein Science* 3: 1984-1991.

Morjana N. A., McKeone B. J., and Gilbert H. F. (1993) Guanidine hydrochloride stabilization of a partially unfolded intermediate during the reversible denaturation of protein disulfide isomerase. *Proceedings of the National Academy of Sciences* 90: 2107-2111.

Murima P., McKinney J. D., and Pethe K. (2014) Targeting bacterial central metabolism for drug development. *Chemistry & Biology* 21: 1423-1433.

Meyer, E., Leonard, N. J., Bhat, B., Stubbe, J., and Smith, J. M. (1992) Purification and characterization of the purE, purK and purC gene products: identification of a previously unrecognized energy requirement in the purine biosynthetic pathway. *Biochemistry* 31: 5022 - 5032.

Myers J. K., Pace C. N., and Scholtz J. M. (1995) Denaturant m values and heat capacity changes: Relation to changes in accessible surface areas of protein unfolding. *Protein Science* 4: 2138-2148.

Nordmann, P., Dortet, L., and Poirel, L. (2012) Carbapenem resistance in *Enterobacteriaceae*: here is the storm! *Trends in Molecular Medicine* 18: 263 - 272.

Pace C. N. (1986) Determination and analysis of urea and guanidine hydrochloride denaturation

curves. *Methods in Enzymology* 131: 266-280.

Pace C. N., Shirley B.A., and Thomson J.A. (1987) Measuring the conformational stability of a protein. Oxford University Press: pp. 311-330.

Pelton, J. T. and L. R. McLean (2000) Spectroscopic methods for analysis of protein secondary structure. *Analytical Biochemistry* 277: 167-176.

Pradeep L. and Udgaonkar J. B. (2004) Effect of salt on the urea-unfolded form of barstar probed by m value measurements. *Biochemistry* 43: 11393-11402.

Royer, C. A. (2006) Probing protein folding and conformational transitions with fluorescence. *Chemical Reviews* 105: 1769 - 1784.

Sainsbury S., Bird L., Rao V., Shepherd S. M., Stuart D. I., Hunter W. N., Owens R. J., and Jingshan Ren J. (2011) Crystal structures of penicillin-binding protein 3 from *Pseudomonas aeruginosa*: comparison of native and antibiotic-bound forms. *Journal of Molecular Biology* 405: 173-184.

Samant S., Lee H., Ghassemi M., Chen J., Cook J. L., Mankin A. S., and Neyfakh A. A. (2008) Nucleotide biosynthesis is critical for growth of bacteria in human blood. *Public Library of Science Pathogens* 4: e37.

Selkoe D. J. (2003) Folding proteins in fatal ways. *Nature* 426: 900-904.

Shortle D. and Meeker A. K. (1986) Residual structure in large fragments of staphylococcal nuclease: effects of amino acid substitutions. *Biochemistry* 28: 936-944.

Strambini G. B. and Gonnelli M. (2010) Fluorescence quenching of buried trp residues by acrylamide does not require penetration of the protein fold. *Journal of Physical Chemistry B* 114: 1089-1093.

Strickland E. H. and Beychok S. (1974) Aromatic Contributions To Circular Dichroism Spectra Of Protein. *CRC Critical Reviews in Biochemistry* 2: 113-175.

Sullivan K. L., Huma L. C., Mullins E. A., Johnson M. E., and Kappock T. J. (2014) Metal stopping reagents facilitate discontinuous activity assays of the de novo purine biosynthesis enzyme PurE. *Analytical Biochemistry* 452: 43–45.

Sun F., Zhou L., Zhao B.-C., Deng X., Cho H., Yi C., Jian X., Song C.-X., Luan C.-H., Bae T., Li Z., and He C. (2011) Targeting MgrA-mediated virulence regulation in *Staphylococcus aureus*. *Chemistry & Biology* 18: 1032–1041.

Tallmadge D. H., Heubner J. S., and Borkman R. F. (1989) Acrylamide quenching of tryptophan photochemistry and photophysics. *Photochemistry and Photobiology* 49: 381-386.

Teague S. J. (2003) Implications of protein flexibility for drug discovery. *Nature Reviews Drug Discovery* 2: 527-541.

Tranchimand S., Starks C. M., Mathews I. I., Hockings S. C., and Kappock T. J. (2011) *Treponema denticola* PurE is a bacterial AIR carboxylase. *Biochemistry* 2011: 4623–4637.

Vivian J. T. and Callis P. R. (2001) Mechanisms of tryptophan fluorescence shifts in proteins. *Biophysical Journal* 80: 2093-2109.

von Hippel P. H. (2016) Changing the stability of macromolecular surfaces by manipulating the aqueous environment. *Biophysical Journal* 111: 1817–1820.

Webb G. F. (2003) A silent bomb: the risk of anthrax as a weapon of mass destruction. *Proceedings of the National Academy of Sciences* 100: 4355-4356.

Zhang J.-H., Chung T. D. Y., and Oldenburg K. R. (1999) A simple statistical parameter for use in evaluation and validation of high throughput screening assays. *Journal of Biomolecular Screening* 4: 67-73.

Zhang Y., Morar M., and Ealick S.E. (2008) Structural biology of the purine biosynthetic pathway. *Cellular and Molecular Life Sciences* 65: 3699-3724.

Zhao A., Tsechansky M., Ellington A. D., and Marcotte E. M. (2013) Revisint and revising the purinosome. *Molecular BioSystems* 10: 369-374.

CURRICULUM VITAE

Anna Kim Jones

SES 4500, M/C 111 845 West Taylor Street Chicago, IL 60607 | 312-848-4384 |

akim94@uic.edu

Education

Doctor of Philosophy, University of Illinois at Chicago, Chicago, IL

2011 - Present

PhD in Chemistry, GPA 3.600

Non-degree program, Japan Center for Michigan Universities, Shiga Prefecture, Japan 2008

Studied Japanese language intensively at Japanese-Language Proficiency Test level of N2 (The ability to understand Japanese used in everyday situations, and in a variety of circumstances to a certain degree)

Bachelor of Science, Calvin College, Grand Rapids, MI 2005 - May 2011

BS in Biology and Biochemistry, GPA 3.637

Experience

Teaching assistant 2008, 2011 - 2016

- Managed operation and grading of laboratory experiments for 40 students per semester
Research assistant 2011 – 2016
- Participated in project to identify 6 small molecule inhibitors for *Bacillus anthracis* 5-carboxyamino imidazole ribonucleotide mutase (BaPurE) with antimicrobial activity in cross-institutional collaboration including Loyola University Medical Center
- Experimental data organization, analysis, presentation and manuscript writing
- Manage undergraduate students through a mini research projects, proposed research plan for incoming undergraduate students for summer research, 2016
- Present research findings at 4 conferences to 50+ experts from academia and graduate students

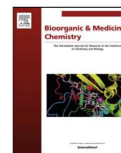
Publications

- Identification of *Bacillus anthracis* PurE Inhibitors with Antimicrobial Activity. Anna Kim, Nina M. Wolf, Tian Zhu, Michael E. Johnson, Jiangping Deng, James L. Cook, Leslie W.-M. Fung. *Bioorganic & Medicinal Chemistry* 23.7 (2015): 1492-1499.
- The *Drosophila* Muller F elements maintain a distinct set of genomic properties over 40 million years of evolution. Leung W, ...Anna Kim,... [Total 940 student co-authors, 74 faculty co-authors] (2015) In press, *G3: GENES, GENOMES, GENETICS*. G3 g3.115.017038.

APPENDIX A

Identification of *Bacillus anthracis* PurE Inhibitors with Antimicrobial Activity.

Anna Kim, Nina M. Wolf, Tian Zhu, Michael E. Johnson, Jiangping Deng, James L. Cook, Leslie W.-M. Fung. *Bioorganic & Medicinal Chemistry* 23 (2015): 1492-1499.



Identification of *Bacillus anthracis* PurE inhibitors with antimicrobial activity



Anna Kim^{a,†}, Nina M. Wolf^{a,†}, Tian Zhu^b, Michael E. Johnson^b, Jiangping Deng^c, James L. Cook^c, Leslie W.-M. Fung^{a,*}

^aDepartment of Chemistry, University of Illinois at Chicago, 845 W. Taylor Street, Chicago, IL 60607, United States

^bCenter for Pharmaceutical Biotechnology, University of Illinois at Chicago, Chicago, IL 60607, United States

^cLoyola University Medical Center, Maywood, IL 60153, United States

ARTICLE INFO

Article history:

Received 12 December 2014

Revised 28 January 2015

Accepted 6 February 2015

Available online 16 February 2015

Keywords:

High-throughput screening

De novo purine biosynthesis

PurE

Thermal shift assay

Sypro Orange

2-Carboxamido-1,3,4-oxadiazole

ABSTRACT

N⁵-carboxy-amino-imidazole ribonucleotide (N⁵-CAIR) mutase (PurE), a bacterial enzyme in the *de novo* purine biosynthetic pathway, has been suggested to be a target for antimicrobial agent development. We have optimized a thermal shift method for high-throughput screening of compounds binding to *Bacillus anthracis* PurE. We used a low ionic strength buffer condition to accentuate the thermal shift stabilization induced by compound binding to *Bacillus anthracis* PurE. The compounds identified were then subjected to computational docking to the active site to further select compounds likely to be inhibitors. A UV-based enzymatic activity assay was then used to select inhibitory compounds. Minimum inhibitory concentration (MIC) values were subsequently obtained for the inhibitory compounds against *Bacillus anthracis* (ΔANR strain), *Escherichia coli* (BW25113 strain, wild-type and ΔTolC), *Francisella tularensis*, *Staphylococcus aureus* (both methicillin susceptible and methicillin-resistant strains) and *Yersinia pestis*. Several compounds exhibited excellent (0.05–0.15 μg/mL) MIC values against *Bacillus anthracis*. A common core structure was identified for the compounds exhibiting low MIC values. The difference in concentrations for inhibition and MIC suggest that another enzyme(s) is also targeted by the compounds that we identified.

© 2015 Elsevier Ltd. All rights reserved.

1. Introduction

Among bacterial pathogens, an increased concern exists for organisms that can be used for bioterrorism, such as *Bacillus*

anthracis (*B. anthracis*), which causes anthrax infection. Due to constant bacterial mutations, with some mutations leading to drug resistance, new antibiotics are urgently and constantly needed.

In many bacterial species (including *B. anthracis*) the *de novo* purine biosynthesis pathway enzyme PurK (also known as N⁵-carboxy-amino-imidazole ribonucleotide (N⁵-CAIR) synthetase) converts 5-amino-imidazole ribonucleotide (AIR) to N⁵-CAIR. PurE (N⁵-CAIR mutase) then converts N⁵-CAIR to 4-carboxy-amino-imidazole ribonucleotide (CAIR).^{1,2} Figure 1 in Ref. 1 and Figures 1 and 2 in Ref. 2 show the pathway and structures of molecules involved. In humans, the enzyme in Step 6 of the pathway (hPur6, also known as AIR carboxylase or PurE II,² or phosphoribosylaminoimidazole carboxylase;³ an enzyme containing a PurE domain) converts AIR and CO₂ to CAIR directly.³ The architecture of the active sites of bacterial PurE and the PurE domain in hPur6 are nearly superimposable, and yet despite these conserved features, biochemical studies have shown that both enzymes are highly specific.⁴ Subsequent studies have shown that bacterial PurE has the potential to be a target for new antibiotic development.⁵

Abbreviations: A₂₆₀, UV absorbance at 260 nm; AIR, 5-amino-imidazole ribonucleotide; Ba, *Bacillus anthracis* (ΔANR strain); CAIR, 4-carboxy-amino-imidazole ribonucleotide; CD, circular dichroism; DMSO, dimethyl sulfoxide; *E. coli* ΔTolC, *E. coli* efflux pump knockout strain; GST, glutathione-S-transferase; hPur6, human enzyme containing a PurE domain, also known as AIR carboxylase; HTS, high-throughput screening; LC1–6, compound names; MIC, minimum bactericidal concentration; MIC, minimum inhibitory concentration; MRSA, methicillin-resistant *Staphylococcus aureus*; MSSA, methicillin-susceptible *Staphylococcus aureus*; N⁵-CAIR, N⁵-carboxy-amino-imidazole ribonucleotide; NAIR, 4-nitro-5-amino-imidazole ribonucleotide; PBS, 5 mM phosphate buffer with 150 mM NaCl at pH 7.4; RRC, Research Resource Center; PurE, N⁵-carboxy-amino-imidazole ribonucleotide mutase; T_m, Boltzmann transition temperature in thermal unfolding; T_m^E, the average T_m value of BaPurE; T_m^{EC}, the average T_m value of replicate runs of BaPurE with a particular compound added; ΔT_m, T_m^{EC} – T_m^E; Tris-25, 25 mM Tris buffer at pH 8; Tris-50, 50 mM Tris buffer at pH 8; UIC, University of Illinois at Chicago.

* Corresponding author. Tel.: +1 312 355 5516.

E-mail address: lfung@uic.edu (L.W.-M. Fung).

† These two authors contributed equally in this work.

<http://dx.doi.org/10.1016/j.bmc.2015.02.016>

0968-0896/© 2015 Elsevier Ltd. All rights reserved.

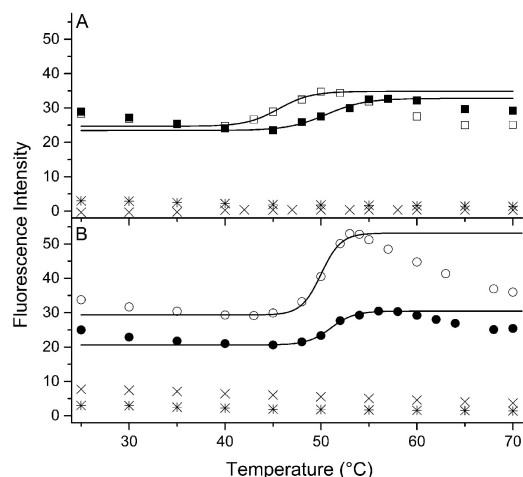


Figure 1. A typical run of thermal unfolding of *BaPurE* (10 μ M) in paired samples (with 100 μ M NAI—filled symbols, or without—empty symbols), monitored by fluorescence intensity of Sypro Orange (5 \times final concentration) at 563 nm (excitation at 490 nm), shows a 5.0 $^{\circ}$ C difference in the transition temperatures, ΔT_m , in Tris-25 (25 mM Tris at pH 8.0) (A). The individual T_m values were obtained from fitting a 2-state unfolding model (solid lines), using only results where fluorescence intensities were increasing with increasing temperatures. It is an indication of protein aggregation when fluorescence intensity decreases as temperature increases.^{5,6} The average ΔT_m in Tris-25 was 5.2 $^{\circ}$ C ($n = 2$). A ΔT_m of 1.0 $^{\circ}$ C is shown for one sample of NAI in Tris-50 (50 mM Tris at pH 8.0) (B). The average ΔT_m in Tris-50 was 1.7 $^{\circ}$ C ($n = 6$). Also shown in the figure are results of samples without *BaPurE*, but with only 5 \times Sypro Orange (\times), or with 10 mM NAI and 5 \times Sypro Orange ($*$), exhibiting little fluorescence signal. The low ionic strength buffer condition (Tris-25) accentuates the thermal shift of *BaPurE* upon compound binding.

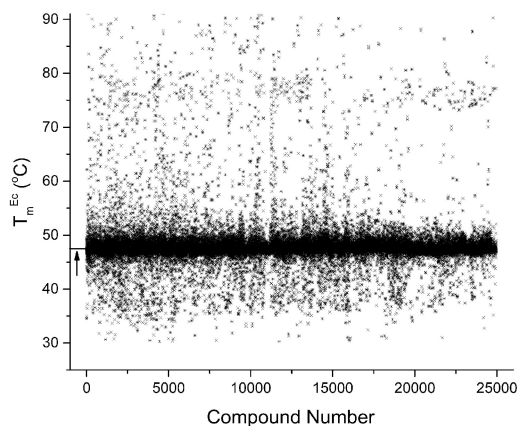


Figure 2. The thermal unfolding transition temperatures of *BaPurE* in the presence of compounds from an antibacterial focused chemical library (24,917 compounds) (T_m^{EC}) in Tris-25, of replicate runs (\times for run 1 and $*$ for run 2). The T_m value of *BaPurE* without a compound (T_m^E) was 47.6 $^{\circ}$ C \pm 0.6 $^{\circ}$ C ($n = 4878$) and is shown as a short dash on the left (noted with an arrow underneath the dash). Ten thousand and nineteen (10,019) compounds exhibited replicate T_m^{EC} values that were within 1.0 $^{\circ}$ C of each other. Five hundred and twenty five (525) compounds with ΔT_m ($T_m^{EC} - 47.6$) in the range of 1.0–20.0 $^{\circ}$ C were selected as hits. See text for details.

In this study, a fluorescence-based⁶ thermal shift assay^{7,8} was applied to *B. anthracis* PurE (*BaPurE*) for high-throughput screening (HTS) to identify molecules (hits) that bind to *BaPurE*. In silico docking was used to select those most likely to bind to the active site. The top scoring molecules were then assayed for inhibitory activity toward *BaPurE*. A few selected inhibitors were used to obtain the minimum inhibition concentration (MIC) against *B. anthracis* (Δ ANR strain), *Escherichia coli* (both the wild-type BW25113 strain and a strain with a *TolC* efflux pump knock out—*E. coli* Δ TolC⁹), *Francisella tularensis* (*F. tularensis*), *Staphylococcus aureus* (*S. aureus*; both methicillin-susceptible (MSSA) and methicillin-resistant strains (MRSA)), and *Yersinia pestis* (*Y. pestis*). MIC values against *B. anthracis* of 0.5–0.15 μ g/mL were obtained for several compounds. A common core structure was identified for compounds with low MIC values. The difference in concentrations for inhibition and MIC suggest that other protein/enzyme molecules are also targeted by the compounds that we identified.

2. Materials and methods

2.1. Chemicals

All materials were purchased from Fisher Scientific (Hampton, NH) unless otherwise noted.

2.2. *BaPurE* plasmid

The *BaPurE* gene (BA0288) from *B. anthracis* (Δ ANR) cells (GenBank: AE017334.2) was inserted into a Gateway pDEST-15 plasmid (Life Technologies; Grand Island, NY) to express an N-terminal glutathione-S-transferase (GST) fusion protein, with a linker between GST and *BaPurE*. In the linker sequence (PWSNQTSLYK-KAGSLVPRGSH), a thrombin cleavage site (the underlined residues) was included. The plasmid was transformed into *E. coli* BL21-CodonPlus (DE3) competent cells (Stratagene; Santa Clara, CA).

2.3. Expression, purification and characterization of *BaPurE*

Cells were grown in a fermentor (Bioflo 110; New Brunswick Scientific, Enfield, CT) containing Terrific broth (2 L) with ampicillin (0.3 mM) at 37 $^{\circ}$ C for 3 h and reduced to 25 $^{\circ}$ C for isopropyl- β -galactoside (1 mM; Gold Biotechnology; St. Louis, MO) induced protein expression for 4 h. The GST-*BaPurE* fusion protein in 5 mM phosphate buffer with 150 mM NaCl at pH 7.4 (PBS) was purified with a glutathione affinity column (Sigma; St. Louis, MO), following standard procedures.^{10,11} Bovine thrombin (Biopharm; Bluffdale, UT) was used to cleave the fusion protein (1 unit thrombin for 1 mg fusion protein). GST and uncleaved fusion protein, if any, in the mixture were removed with the affinity column again, to give *BaPurE*. An extinction coefficient of 11,460 mol⁻¹ cm⁻¹, obtained from the amino acid sequence, was used to determine protein concentration for the monomer. The integrity of the protein was checked with sodium dodecyl sulfate polyacrylamide gel electrophoresis and high-resolution/high-mass mass-spectrometry, using a LTQ-FT spectrometer in the Research Resources Center at the University of Illinois at Chicago (UIC). The *BaPurE* sample was concentrated to 150 μ M (2.6 mg/mL) and frozen dropwise, about 20 μ L per drop, in liquid nitrogen for storage at -80° C.

We selected the GST fusion protein over the commonly used His-tag fusion protein to prepare *BaPurE* to avoid introducing high concentrations of imidazole, a heterocyclic compound somewhat similar to the substrate, which may be difficult to remove from the protein. Additionally, a His-tag *BaPurE* protein was initially prepared by standard procedures¹² in 50 mM Tris buffer at pH 7.8 with NaCl and imidazole, 500 mM each. However, following

dialysis of protein (at a concentration of 50–350 μM or 1–7 mg/mL) in 50 mM Tris buffer at pH 7.8 with NaCl and imidazole, 50 mM each, only about 20% protein remained soluble.

The oligomeric state of BaPurE in solution was determined by gel filtration with a Superdex 200 GL column and an FPLC system (AKTApurifier, GE Healthcare Life Sciences; Pittsburgh, PA). A calibration curve of molecular mass and elution volume was obtained with ferritin, aldolase, conalbumin, chymotrypsinogen A, ribonuclease A and blue dextran (GE Healthcare Life Sciences).

The secondary structure of BaPurE (25 μM) in PBS buffer or Tris (25 mM) buffer at pH 8 (Tris-25) at 25 $^{\circ}\text{C}$ was determined from circular dichroism (CD) spectra obtained with a CD spectrometer (Model 810; Jasco; Oklahoma City, OK), and K2D3 software (<http://k2d3.org.ca>).¹³ The secondary structure from the X-ray structure (PDB code: 1XMP,¹⁴) was obtained for comparison, using PDBsum (<http://www.ebi.ac.uk/pdbsum/>).¹⁵

2.4. Enzyme activity

The published method for assaying PurE¹ was applied to BaPurE. Briefly, the conversion of CAIR to N⁵-CAIR in this reversible reaction of PurE was monitored by measuring the UV absorbance at 260 nm (A_{260}) for 1.5 min at 20 $^{\circ}\text{C}$. CAIR was prepared in house following published methods,¹⁶ involving the use of LiOH to saponify aminoimidazole-4-carboxamide ribonucleotide to give CAIR in high yield (85%) and purity (99%). The K_m value for CAIR in BaPurE was determined as 9.7 μM . The reported K_m value for CAIR in *E. coli* PurE under their experimental condition is reported as 22 μM ¹⁷ or 36 μM .¹⁸ The CAIR stock solution (5 mM) was prepared in 50 mM Tris buffer at pH 8.0 (Tris-50) and stored at -80°C in 100 μL portions, and a working solution of CAIR (60 μM), prepared in Tris-25, was stable with no change in A_{260} for at least 2 h. For the assay sample, equal volumes of BaPurE and CAIR were mixed to give 10 nM BaPurE and 30 μM CAIR in Tris-25. Assay samples consisting of 10 μM CAIR were also prepared. Dimethyl sulfoxide (DMSO, 1%) was included such that the samples were similar to those used in enzyme inhibition assays (Section 2.8). The linear portion of the A_{260} versus time plot was fitted to give a $\Delta A_{260}/\Delta t$ value (the initial rate) (see Fig. 4, for example). CAIR concentration was calculated from a $\Delta \varepsilon_{260}$ of $8930 \text{ M}^{-1} \text{ cm}^{-1}$,¹⁹ and was used to determine the specific activity, which was defined¹⁸ as the disappearance of 1 μmol of CAIR in 1 min with 1 mg of PurE (unit/mg). The $\Delta \varepsilon_{260}$ was used since N⁵-CAIR in acidic pH is known to undergo auto-decarboxylation to form AIR, but the rate of the decomposition is minimal at pH 8.0.¹⁸

2.5. Optimization for thermal shift screening

Sypro Orange (Invitrogen; Life Technologies; Carlsbad, CA), used for thermal unfolding,⁷ was supplied as a 5000 \times stock solution in anhydrous DMSO, and stored in a desiccator at 4 $^{\circ}\text{C}$. The hygroscopic DMSO absorbs moisture during the freeze–thaw process, and when DMSO contains more than 5% water, it does not freeze at 4 $^{\circ}\text{C}$.²⁰ Thus, we minimized the number of freeze–thaw cycles of the stock solution, and discarded stock samples when they became liquid at 4 $^{\circ}\text{C}$.

The initial studies for optimizing the conditions for thermal unfolding of BaPurE to be used for high-throughput assay were monitored with a fluorescence spectrometer (Jasco FP-6200), with Sypro Orange excitation at 490 nm and emission at 563 nm. The buffer conductivity values were measured with a conductivity meter (Yellow Springs model 31; Yellow Springs, OH) to ensure consistency in buffer conditions with different preparations. The conductivity value of Tris-25 was 1200 μMHO ; for Tris-50 it was 2600 μMHO ; and for PBS it was 13,000 μMHO . The fluorescence emission intensities for samples of BaPurE (10 μM) in different buf-

fers with 5–15 \times Sypro Orange and 1% DMSO were measured from 25 to 75 $^{\circ}\text{C}$. A known inhibitor, 4-nitro-5-amino-imidazole ribonucleotide (NAIR),⁴ at 100 μM , was used to evaluate whether the compound-binding-induced stability in BaPurE was detectable by the thermal shift method. Samples without BaPurE, but with only Sypro Orange and NAIR, or with only Sypro Orange were also prepared. NAIR, also called NO₂-AIR,¹⁷ was synthesized in house as described.²¹ The thermal unfolding data were fitted to a two-state transition model to give Boltzmann transition temperatures.

2.6. High-throughput thermal shift screening

BaPurE samples from different preparations, a total of about 100 mg, were combined and dialyzed in the buffer identified in optimization studies (Tris-25; from Section 3.2). An antibacterial focused chemical library of 24,917 compounds (Life Chemicals; Burlington, Canada)²² was screened. Compounds (10 mM) in anhydrous DMSO were stored in 384-well plates at -80°C with desiccation. All components (10 μM BaPurE in Tris-25 with 5 \times Sypro Orange, a condition determined from the results obtained in optimization studies (from Section 3.2), 100 μM compound and 1% DMSO) were delivered to each well in the 384-well white plates (ABgene SuperPlate, Fisher Thermo Scientific) by a liquid handling system (Freedom Evo, Tecan; Mannedorf, Switzerland). A total of 78 plates were used per run, and replicate runs were done. For each plate, 32 wells were reserved for samples (1) with only Sypro Orange and DMSO (no BaPurE and compound) to monitor the background fluorescence, and (2) with BaPurE, Sypro Orange and 1% DMSO (no compound) to monitor signals from the control samples. For two plates 32 wells were reserved for samples with 100 μM NAIR, as positive control. Plates were covered with plastic film (Applied Biosystems, Foster City, CA) and stored at 4 $^{\circ}\text{C}$.

The first plate, within 10–30 min after it was prepared, was removed from storage and placed in a RT-PCR instrument (ViiA7 RT-PCR; Applied Biosystems, Carlsbad, CA) for thermal unfolding measurements over a temperature range of 25–95 $^{\circ}\text{C}$ at a rate of 0.075 $^{\circ}\text{C}/\text{s}$. An instrument filter with emission at $586 \pm 10 \text{ nm}$ and excitation at $470 \pm 15 \text{ nm}$ was used. The measurements were done continuously. A replicate run followed immediately after the first run. All operations and measurements were done in the Research Resource Center (RRC) at UIC.

The thermal unfolding profiles were analyzed with the Protein Thermal Shift Software (Applied Biosystems) to determine the Boltzmann transition temperature, T_m . Compounds with T_m values in replicate runs that differed by more than 1.0 $^{\circ}\text{C}$ were eliminated, since our standard deviation values for T_m values of BaPurE was 0.6 ($n = 4878$; from Section 3.3). The average T_m value of the control (BaPurE) (T_m^E) and the average value of replicate runs of compound (T_m^C) were used to determine thermal shift values ($\Delta T_m = T_m^C - T_m^E$). Hits were defined as those with $1.0^{\circ}\text{C} < \Delta T_m < 20.0^{\circ}\text{C}$. We used 20.0 $^{\circ}\text{C}$ as the upper cut-off since most of the thermal shift values in the literature are less than 20 $^{\circ}\text{C}$ (e.g.,^{23–25}). The thermal shift value for our positive control (NAIR) was 5.6 $^{\circ}\text{C}$ (from Section 3.3). This selection criterion may obviously eliminate a fraction of molecules that bind to BaPurE, but is more time and cost efficient as well as providing more reliable hits.

The Z'-factor²⁶ used to evaluate the quality of the thermal shift assay was determined from the average T_m values of BaPurE, in the absence (T_m^E) and in the presence of 100 μM NAIR (T_m^C (NAIR)), and their corresponding standard deviation (SD) values, as $1 - 3 \{ (T_m^C \text{ (NAIR)} + T_m^E) / (SD \text{ (NAIR)} - SD \text{ (BaPurE)}) \}$.

2.7. Docking to active site

The SMILES strings of hits were converted, using LigPrep (Schrödinger), to their 100 most energetically and structurally

favorable structures. All structures were also clustered and selected with Canvas (Schrödinger) for structural diversity. GOLD v5.0.1 (Cambridge Crystallographic Data Centre; Cambridge, United Kingdom) was used for docking the structures of each compound to PurE. We did not use the published structure of BaPurE (PDB: 1XMP) since it does not contain a ligand, instead we used the structure of *E. coli* PurE with AIR (PDB: 1D7A), with AIR removed. The AIR binding site was assumed to be the active site, or part of the active site, and a binding site sphere with a radius of 10 Å centered on AIR was used. Standard default settings were used for other parameters, such as full solvation, retaining the three top solutions, and no force constraints.

2.8. Enzyme inhibition

Each compound (20 μM) and BaPurE (20 nM) was incubated in Tris-25 for 1.5 min at 20 °C, followed by addition of an equal volume of CAIR to give an assay sample consisting of compound (10 μM), BaPurE (10 nM) and CAIR (30 μM) in Tris-25 with 1% DMSO. A control sample (without the compound) was prepared in parallel. Assay samples with CAIR concentration the same as compound concentration (10 μM) were also tested. A_{260} was measured as a function of time, and BaPurE activity inhibitions were determined as [(activity with compound)/(activity without compound) × 100].

Only compounds with masses validated by mass spectrometry analysis were used. To avoid compound aggregation and stability problems due to freeze–thawing,^{27,28} the compounds in DMSO were stored at room temperature under desiccation. We noted that some compounds precipitated out when pipetted into Tris-25; those were eliminated from further study. Compounds in Tris-25 that exhibited increasing or decreasing A_{260} readings as a function of time were also eliminated. No particular actions were taken for those compounds exhibiting a constant A_{260} value since the absorption only added to the baseline. Triton X-100 (0.01–0.1%) was included in some assay solutions to check for compound aggregation induced inhibition. Compound concentration of stock solutions was determined by weight and volume, which may introduce uncertainties.²⁹

2.9. Minimum inhibitory concentration (MIC) and minimum bactericidal concentration (MBC)

MIC was determined as in prior work.³⁰ Briefly, the MICs of compounds were tested against *B. anthracis* (ΔANR strain), *E. coli* (BW25113 strain, WT and ΔTolC), *F. tularensis* (BEI/ATCC: UTAH 112), two strains of *S. aureus*, one methicillin-sensitive (ATCC: 29213) and one *mecA*-positive, methicillin-resistant (ATCC: 43300), and *Y. pestis* (BEI/ATCC: A1122). LB medium was added to each well in a row of a sterile 96-well flat bottom tissue culture plate, with 96 μL to the first column and 50 μL to all subsequent wells. The inhibitors to be tested were added to the first column to give a final well volume of 100 μL. Inhibitors were then serially diluted (2-fold) across the columns of wells by pipetting and mixing 50 μL of solution. The extra 50 μL was discarded from the final well. Ciprofloxacin, a commercial antibiotic used for the treatment of a number of bacterial infections, was used as positive control in these studies. Prior to setting up the MIC plates, the appropriate bacterial cultures were grown to mid-log phase and subsequently diluted to an optical density reading at 600 nm of 0.004 with fresh LB medium. This bacterial dilution (50 μL) was added to each well of the plate, and the plate was then incubated at 37 °C overnight without shaking. For each inhibitor the first clear well with no signs of visible growth was reported as the MIC value. All MIC values were confirmed by at least two independent titrations.

MBC values were estimated using the standard method of testing all negative MIC wells (no visible growth) for evidence of viable bacteria by transferring an aliquot of MIC dilution culture media to antibiotic-free agar plates. Medium (100 μL) from each negative (clear) well in MIC assays was streaked onto LB agar plates, and the plates were incubated for 72 h for detection of bacterial growth. The MBC of an inhibitor was defined as the highest MIC assay dilution that resulted in no growth of bacteria during this sub-cultivation. Bactericidal activity was defined as an MBC/MIC ratio ≤4. Since the highest compound concentration tested was 12.5 μg/mL, clear statements about bacteriostatic versus bactericidal activity could only be made about inhibitors with MICs ≤3.13 μg/mL.

3. Results

3.1. Protein properties

About 15 g of cells were obtained from 2 L of medium, and about 0.5 mg recombinant BaPurE (>85% pure) was obtained from 1 g of cells with 80–90% purity, as indicated by sodium dodecyl sulfate gel electrophoresis. Mass spectrometry results showed a mass of 17,322.1 Da, with the expected mass from sequence of 17,322.9 Da, confirming the integrity of BaPurE. In PBS, the protein, up to ~1.7 mM (~30 mg/mL), remained soluble in its native form as an octomer, as indicated by the hydrodynamic mass of 149 kDa from gel filtration measurements.

CD spectra of BaPurE in PBS and in Tris-25 at 25 °C showed a secondary structure with about 24% beta sheet and 32% alpha helix, indicating well folded protein samples. Slightly higher helical and lower sheet contents were obtained for buffers with higher salt concentrations (Wolf and Fung, unpublished data). The secondary structure content calculated from the X-ray structure (PDB: 1XMP) is 15% beta sheet and 45% alpha helix.

For enzyme activity, the average $\Delta A_{260}/\Delta t$ value in Tris-25 at 20 °C was 0.0115 ± 0.0012 ($n=21$) to give a specific activity of 7.5 ± 0.8 unit/mg. The value varied in other buffers: 10.6 ± 1.6 unit/mg ($n=13$) in Tris-50, and 12.4 ± 1.3 unit/mg ($n=24$) in PBS. These values differ from those of PurE from other species under different solution conditions.^{17–19}

3.2. Optimal condition for thermal shift screening

Sypro Orange at 5× concentration with or without NAIR, but with no BaPurE, exhibited little changes in the fluorescence intensity as a function of temperature in either Tris-25 (Fig. 1A) or Tris-50 (Fig. 1B). In Tris-25, a typical thermal unfolding profile of BaPurE (10 μM), with 5× Sypro Orange and 1% DMSO, showed a prominent thermal transition, with a T_m^E value of 45.6 °C, and was shifted to 50.6 °C in the presence of NAIR (100 μM), to give a change in the T_m value (ΔT_m) of 5.0 °C for this particular run (Fig. 1A). In Tris-50, the T_m^E value was higher (50.0 °C), but was shifted only to 51.0 °C in the presence of NAIR to give a ΔT_m of 1.0 °C in this paired run (Fig. 1B). The average thermal shift for NAIR in Tris-25 was 5.2 ± 0.3 °C ($n=2$), and in Tris-50 was 1.7 ± 0.9 °C ($n=6$). Thus, BaPurE in Tris-25 exhibited a larger thermal shift than in Tris-50, and Tris-25 was selected for HTS. Three Sypro Orange concentrations, 5×, 10× and 15×, yielded satisfactory thermal unfolding profiles for BaPurE in Tris-25, and the lowest concentration, 5×, was selected for HTS.

3.3. High-throughput thermal shift screening

From the conditions identified above, the high-throughput thermal shift screening samples consisted of BaPurE at 10 μM in Tris-25 with 5× Sypro Orange and 1% DMSO.

From HTS thermal shift measurements, the average T_m^{EC} was found to be $47.8 \pm 0.3^\circ\text{C}$ ($n = 32$), and the T_m^{EC} (NAIR) was $53.4 \pm 0.5^\circ\text{C}$. The Z'-factor was calculated as 0.57, indicating the set-up provided reliable thermal shift results.

The average T_m^{EC} obtained from all the control wells in all plates, was $47.6 \pm 0.6^\circ\text{C}$ ($n = 4878$) (Fig. 2). For the samples with compounds (24,917 compounds) (Fig. 2), 10,019 samples displayed a difference in $T_m^{\text{EC}} < 1.0^\circ\text{C}$ between replicate runs, and were used for further analysis. The remaining samples (14,898 samples) were eliminated. Based on the T_m selection criteria for hits discussed in Section 2.6 as $1.0^\circ\text{C} < \Delta T_m < 20.0^\circ\text{C}$, compounds exhibiting $\Delta T_m (=T_m^{\text{EC}} - 47.6)$ values outside the range of $1\text{--}20^\circ\text{C}$ were not considered. Thus 197 samples with negative ΔT_m , 9257 with less than 1°C in ΔT_m and 40 with ΔT_m larger than 20°C were not considered further. The remaining samples (525 compounds) satisfied the selection criteria.

3.4. Active site docking selection

The docking of 525 thermal shift hits to the AIR binding site sphere yielded 79 compounds with GOLD docking scores greater than or equal to 55. Both CAIR and NAIR gave a docking score of 56. Compound diversity selection (discussed in Section 2.7) further narrowed the list to 60 compounds. Two of these compounds are shown in the active site, with AIR in the center of the cavity (Fig. 3). The active site appears to be relatively open and spacious, with ample space for a hit to bind. With one of these hits in the active site, the substrate $\text{N}^5\text{-CAIR}$ (similar in size to AIR) would be blocked from entering the active site.

3.5. Inhibition activity

Of the 60 selected compounds, 16 compounds, at $10\text{ }\mu\text{M}$, exhibited 6% to 27% inhibition of the activity of *BaPurE* (10 nM) in Tris-25 at 20°C (Tables 1 and 3). We found that the inhibition values did not depend on whether 10 or $30\text{ }\mu\text{M}$ CAIR was used. In a typical paired run under the same condition, the known inhibitor NAIR reduced the activity by 21%, whereas **LC1** inhibited by 30% (Fig. 4).

The inhibition assay results of samples with and without $0.1\text{--}0.01\%$ Triton X-100 were generally similar. For example, for **LC3** without Triton the average was $13 \pm 4\%$, and with Triton it was $12 \pm 3\%$; for **LC5** without Triton it was $20 \pm 5\%$ and with Triton it was $26 \pm 5\%$; and for **LC6** without Triton it was $15 \pm 0\%$ and with

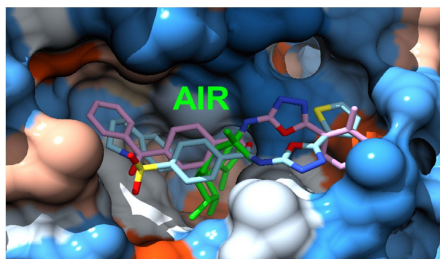


Figure 3. The active site of *EcPurE* with AIR (PDB: 1D7A, Chain B) is displayed. It is colored by amino acid residue hydrophobicity, with blue for the most hydrophilic, to white, to orange-red for the most hydrophobic. AIR (green color) is deep in the binding-site pocket. The residues on the right are K17 and E158 (blue color) and the residue on the left is A96 (beige color). Two representative compounds (**LC1** and **LC3**) are docked in the active site. The active site appears to be relatively open and spacious, with ample space for the compounds. With any of these compounds in the active site, molecules similar in size to AIR would be blocked from entering the active site.

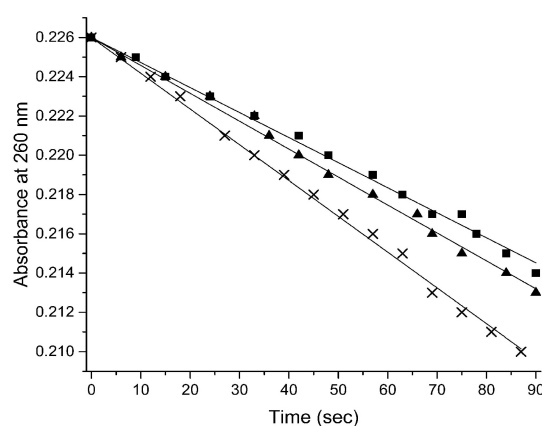


Figure 4. The activity of 10 nM *BaPurE* in Tris-25 (\times) was monitored by the absorbance at 260 nm of $30\text{ }\mu\text{M}$ CAIR. To measure the inhibition activity, **LC1** or NAIR ($20\text{ }\mu\text{M}$) and *BaPurE* (20 nM) was incubated in Tris-25 for 1.5 min at 20°C , following by addition of an equal volume of CAIR to give an assay sample consisting of **LC1** or NAIR ($10\text{ }\mu\text{M}$), *BaPurE* (10 nM) and CAIR ($30\text{ }\mu\text{M}$) in Tris-25 with 1% DMSO. The A_{260} value was monitored for 1.5 min at 20°C ; the linear portion of the plot was fitted to give a $\Delta A_{260}/\Delta t$ value (initial rate). The inhibition activity of **LC1** (filled square) was 30% and of NAIR (filled triangle) was 21% in this paired run. The average inhibition activity for **LC1** was $27 \pm 6\%$ ($n = 3$), and for NAIR was $21 \pm 3\%$.

Triton it was $7 \pm 4\%$. These results indicated that the observed inhibitions were not due to compound aggregation induced inhibition.

3.6. MIC values

MIC assay results (Tables 1 and 3) were highly reproducible. On repeated testing, most were identical, a few differed by twofold, and only 1 differed by fourfold. Five compounds exhibited excellent bacteriostatic antimicrobial activity against *B. anthracis* at a level of $0.05\text{--}0.15\text{ }\mu\text{g/mL}$, which is comparable to the activity of ciprofloxacin ($0.11\text{ }\mu\text{g/mL}$) and better than linezolid ($2\text{ }\mu\text{g/mL}$, from Ref. 31). Higher MIC values were obtained for these compounds when tested against *F. tularensis* than when tested against *B. anthracis*. Thus, four of the compounds had bacteriostatic activity against *F. tularensis* at concentrations ranging from $1.2\text{--}6.3\text{ }\mu\text{g/mL}$, while one compound (**LC3**) had no detectable activity ($\text{MIC} > 12.5\text{ }\mu\text{g/mL}$). Two of the compounds (**LC5** and **LC6**) had detectable bacteriostatic activity against *Y. pestis*, with MICs of $3.1\text{ }\mu\text{g/mL}$, whereas the other three compounds were inactive ($\text{MIC} > 12.5\text{ }\mu\text{g/mL}$) (Table 1).

Comparative testing of these compounds against methicillin-susceptible *S. aureus* (MSSA) and methicillin-resistant *S. aureus* (MRSA) revealed three patterns of activity. One of the compounds (**LC3**) was inactive against both MSSA and MRSA ($\text{MICs} > 12.5\text{ }\mu\text{g/mL}$). Three of the compounds (**LC1**, **LC5** and **LC6**) had excellent activity against MSSA, with MICs of 0.29 , 0.78 and $1.56\text{ }\mu\text{g/mL}$, respectively. These MICs were in a similar range to that of the positive control antibiotic, ciprofloxacin. These compounds also had activity against MRSA that was similar to their activity against MSSA (within a $1\text{--}3$ fold difference), with anti-MRSA MICs of 0.39 , 1.95 and $3.13\text{ }\mu\text{g/mL}$, respectively. The fifth compound (**LC4**) tested against these staphylococcal strains had a unique pattern of activity, when compared with the others. It was highly active against MSSA ($\text{MIC} = 0.20\text{ }\mu\text{g/mL}$) but inactive against MRSA ($\text{MIC} > 12.5\text{ }\mu\text{g/mL}$).

These compounds were also tested against *E. coli* as a representative Gram-negative pathogen. Initial studies revealed that wild

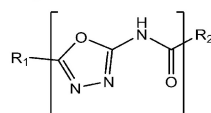
Table 1The thermal shift (ΔT_m) of BaPurE induced by compounds (100 μ M) and inhibitory activity of compounds (10 μ M) toward BaPurE in 25 mM Tris buffer

Compound	ΔT_m^a ($^{\circ}$ C)		Inhibition ^b (%)		MIC (μ g/mL)				
	BaPurE	BaPurE	Ba ^c	Ft ^c	Yp ^c	MSSA ^c	MRSA ^c	Ec Δ TolC ^c	
LC1	2.0	27	0.15	6.25	>12.5	0.29	0.39	0.29	
LC2	7.9	19	0.10	3.1	>12.5	>12.5	6.25	0.39	
LC3	1.9	13	0.10	>12.5	>12.5	>12.5	>12.5	>12.5	
LC4	2.4	19	0.10	6.3	>12.5	0.2	>12.5	0.02	
LC5	1.1	20	0.05	1.6	3.1	0.78	1.95	0.07	
LC6	1.4	15	0.78	1.2	3.1	1.56	3.13	0.39	
NAIR	5.6	24	ND	ND	ND	ND	ND	ND	
Ciprofloxacin	ND ^d	ND	0.11	0.03	0.04	0.35	0.34	0.01	
Linezolid	ND	ND	2 ^e	32 ^f	ND	2 ^g	ND	ND	

Also listed are the MIC values of the compounds against various bacterial strains.

^a $\Delta T_m = T_m^c - T_m^E$, with the average transition temperature for BaPurE (T_m^E) as 47.6 $^{\circ}$ C from high throughput screening, with $n = 4878$. T_m^c values were average values from replicate runs in high-throughput screening. For NAIR, $n = 32$.^b Values were averages, with $n = 2-4$ with the standard deviations $\sim 7\%$.^c Ba = *B. anthracis* (Δ ANR strain) cells; Ft = *F. tularensis* cells; Yp = *Y. pestis* cells; MSSA = *S. aureus* (methicillin susceptible strain 29213) cells; MRSA = *S. aureus* (methicillin-resistant strain 43300) cells; Ec Δ TolC = *E. coli* (BW25113 Δ TolC) cells.^d ND = not determined.^e Ref. 31.^f Ref. 40.^g Ref. 41.**Table 2**

Structures of the inhibitor compounds in Table 1



Compound	R ₁	R ₂
LC1	Thiophene	1-(Toluene-4-sulfonyl)-1,2,3,4-tetrahydro-quinoline
LC2	2,5-Dichlorobenzene	2-Phenylepidine
LC3	2,4-Dimethylbenzene	Benzophenone
LC4	2,5-Dimethylbenzene	3-Chlorobenzene
LC5	2,5-Dimethylbenzene	2,5-Chlorothiophene
LC6	4-Bromobenzene	4-Chloroanisole

These compounds include a core structure of 2-carboxamido-1,3,4-oxadiazole, with the R₁ and R₂ groups noted.

type *E. coli* was highly resistant to these compounds (MIC > 12.5 μ g/mL). However, four compounds were highly active against *E. coli* Δ TolC, with MICs ranging from 0.02 to 0.4 μ g/mL, and one of the compounds (**LC3**) was inactive. Two of the compounds (**LC4** and **LC5**) exhibited activities (MIC of 0.02 and 0.07 μ g/mL, respectively) that were comparable to that of ciprofloxacin (MIC of 0.01 μ g/mL) against *E. coli* Δ TolC.

Table 3The thermal shift (ΔT_m) of BaPurE induced by inhibitors that exhibited large (>12.5 μ g/mL) MIC values for *B. anthracis* (Δ ANR strain), *F. tularensis*, and *Y. pestis*

Compound	BaPurE		SMILES	MIC (μ g/mL)		
	ΔT_m ($^{\circ}$ C)	Inhibition (%)		Ba	Ft	Yp
LC7	5.2	28	BrC1=CC(=CC=C1OC(=O)N1C(=O)OC1=CC=CC1)S(=O)(=O)C1=CC=C2C=CC=C2=C1	>12.5	ND ^a	ND
LC8	1.8	20	FC1=CC(C1)=C(C=C1)C(=O)N1C=CC(=O)NCC2=CC=CC=C2	>12.5	>12.5	>12.5
LC9	3.0	17	COC1=CC(OC)C(=CC=C1)C(=O)N1C=CC(=O)N1C=CC2=CC=C2	>12.5	>12.5	>12.5
LC10	4.4	17	[Br-].CC1=[N+](CC(O)=O)C2=C(S1)C=CS2	>12.5	>12.5	>12.5
LC11	3.1	14	FC(F)(F)C1=CC=CC(NC(=O)N2CCN(CC2)C2=NN3C=NN=C3=C2)=C1	>12.5	>12.5	>12.5
LC12	1.5	12	NS(=O)(=O)C1=CC=C(NC(=O)CSC2=NN=C(O2)C2=CC=CC=C2)C=C1	>12.5	ND	ND
LC13	4.7	11	ClC1=CC=C(C=C1)C1=C(NC(=O)C2=CC=CC2)N2CCSC2=N1	>12.5	>12.5	>12.5
LC14	1.8	7	CCCC(C)CNC1=NC2=C(N1CC(O)COC1=CC=C(C)C(C)=C1)C(=O)N2C	ND	>12.5	ND
LC15	1.2	6	COC1=CC(OC)C(=CC=C1)C1=NC(NC2=NC(C(=O)NCC3=CC=C(C1)C=C3)=C2)N=C(C)O1	>12.5	>12.5	ND

These inhibitors do not have the core structure discussed in the text and shown in Table 2. Samples used both thermal shift and inhibitions were in Tris-25.

^a ND = not determined.

The MBC value against *B. anthracis* for **LC4** was 6.3 μ g/mL and for **LC5** was 0.8 μ g/mL. The values for **LC1**, **LC2**, **LC3**, and **LC6** were >12.5 μ g/mL. For all six compounds (**LC1–LC6**), the MBC/MIC ratios were >4. Thus these compounds exhibited bacteriostatic activity against *B. anthracis*.

3.7. Core structure identification

Six inhibitors exhibited very low MIC values against *B. anthracis* (0.05–0.78 μ g/mL) (Table 1). We found that all six inhibitors contained a common core structure, a 2-carboxamido-1,3,4-oxadiazole (Table 2). The inhibitors that exhibited MIC values >12.5 μ g/mL against *B. anthracis*, *F. tularensis* and *Y. pestis* (Table 3) did not have the same core structure and were not tested against *S. aureus* and *E. coli* Δ TolC.

4. Discussion

N⁵-carboxy-amino-imidazole ribonucleotide mutase (PurE) is an essential enzyme in the *de novo* purine biosynthesis pathway in *B. anthracis*, *F. tularensis*, *S. aureus*, *Y. pestis*, and many other pathogens, and studies have shown it to be a potential target for a new generation of antibiotics.⁵

The standard enzyme assay for PurE is a UV-based assay,^{1,18,19} which is insensitive for high-throughput screening. Thermal shift binding methods have been used to screen for compounds binding

to proteins. However, in 50 mM Tris buffer at pH 8, a buffer condition used in most PurE activity studies,^{1,19} we showed that the thermal shift from a molecule known to bind to PurE, NAIR, was relatively small (1–2 °C). We found that a much larger thermal shift, about 5 °C, was observed for BaPurE in 25 mM Tris buffer at pH 8. With this buffer condition, we identified over 500 compounds in a chemical library of about 25,000 compounds that exhibited 1–20 °C thermal shift and thus as ‘binders’ to BaPurE. These compounds were further selected as potentially binding to the active site, with docking method. Sixty compounds with high docking scores were selected for enzyme activity inhibition measurement, and 15 compounds found to inhibit BaPurE activity. Several compounds exhibited an inhibition activity comparable to that of NAIR. NAIR has been reported to be a tight-binding inhibitor of *Gallus gallus* PurE with a K_i of 0.34 nM but a steady-state inhibitor of *E. coli* PurE with K_i of 0.5 μ M.³²

Six inhibitors also exhibited low MIC values against *B. anthracis* (Δ ANR strain), *E. coli* (BW25113 strain, Δ TolC), *F. tularensis*, *S. aureus*, or *Y. pestis*. Two of these inhibitors exhibited activity against 3 of the 6 Category A biowarfare agents (*F. tularensis*, *B. anthracis* and *Y. pestis*, CDC information) at levels comparable to current commercial antibiotics, presumably through a different (novel) mechanism not utilized by any other commercial antibiotic. The precise molecular mechanism awaits future elucidation. It is interesting to note that the MIC values of the compounds were much lower (about 0.1 μ M for LC5, for example) than the concentration (10 μ M) needed to exhibit inhibition toward BaPurE activity. These results suggest that other protein/enzyme molecules are also targeted by these compounds. Clearly additional studies are warranted for further development of these antimicrobial compounds as potential drug molecules.

These 6 compounds exhibiting low MIC values contain a core structure of 2-carboxamido-1,3,4-oxadiazole. A component of the core structure is the 1,3,4-oxadiazole moiety. Compounds containing the 1,3,4-oxadiazole moiety have been identified in several studies (e.g.,^{33–37}), and reviewed recently.³⁸ Four of the five recently identified inhibitors of *trans*-translation contain the core structure,³⁹ but these four compounds are not the same as the ones identified in this study. As noted previously,³⁴ ‘there are numerous literature examples of the 2,5-disubstituted-1,3,4-oxadiazole system that have shown biological activities including anticancer, anti-inflammatory, antifungal, antiviral, and antibacterial or antimycobacterial activity’. Amongst the compounds with this core structure that have appeared in literature, only one compound described here (LC5) has appeared in literature.³⁴ However, the published studies have not identified detailed mechanism of action of these compounds.

Our studies identified six inhibitors from high-throughput screening with BaPurE that exhibit high-level antimicrobial activity against *B. anthracis* (MIC < 1 μ g/mL). The finding supports the approach of screening compounds for enzyme inhibition activity as a means to identify lead agents with antimicrobial activity. Some of the compounds had cross-strain activity against *F. tularensis* and *Y. pestis*, but with MIC values that were ~10 times higher than those for *B. anthracis*. The reduction in activity against these species is perhaps a consequence of limited cell penetration or differential efflux.

Some of the compounds had cross-strain activity against *S. aureus*, in some cases with MICs < 1 μ g/mL. These results suggest that these compounds might represent a new class of antimicrobial agents that could be studied and developed for anti-staphylococcal activity. This possibility is much more important for the compounds with anti-MRSA activity (see below), since the clinical options for treating MRSA infections are limited.

Three of the compounds that had anti-Staph (MSSA) activity had nearly comparable activity against MRSA. In contrast, one of

the compounds (LC4) had high-level bacteriostatic activity against MSSA (MIC = 0.2 μ g/mL) but was inactive against MRSA (MIC > 12.5 μ g/mL). These observations raise interesting questions about the mechanisms of action of the compounds that were active against MRSA and even more interesting questions about the compound structure–function related differences that might explain the high-level resistance of MRSA to LC4.

The high-level activity of some of these compounds against the *E. coli* efflux pump knockout strain (Δ TolC) (MIC values between 0.02 and 0.39 μ g/mL) indicate that the target in some Gram-negative bacteria is sensitive to some of these inhibitors. Further testing of efflux pump competent (wild-type) strains of *E. coli* and of other Gram-negative bacteria will be required to determine the extent of inhibitory activity and the limitations of compound efflux and to consider means of evading efflux-mediated resistance in *E. coli*.

5. Conclusion

Among bacterial pathogens, an increased concern exists for organisms that can be used for bioterrorism, such as *Bacillus anthracis* (*B. anthracis*), which causes anthrax infection. Due to constant bacterial mutations, with some mutations leading to drug resistance, new antibiotics are urgently and constantly needed. We used a low ionic strength buffer condition to accentuate the thermal shift values of BaPurE upon binding compounds from an antibacterial focused chemical library of 24,917 compounds. From the binding compound list, we applied in silico docking to reduce hits to 60 compounds for enzyme activity measurements. 15 inhibitors were identified and six exhibited high-level antimicrobial activity against *B. anthracis* (Δ ANR strain) (MIC < 1 μ g/mL). These compounds also exhibited low MIC values against *E. coli* Δ TolC, *F. tularensis*, *S. aureus* (MSSA and MRSA), and *Y. pestis*. The compounds with low MIC values all contained a core structure of 2-carboxamido-1,3,4-oxadiazole. It should be noted that with the concentrations needed for BaPurE inhibition being much higher than MIC values, our study also suggest that other protein/enzyme molecules are being targeted by these compounds. With the low MIC values, we believe that these compounds are well-suited for further studies on the molecular mechanism of their antimicrobial action and for future synthetic improvement to enhance antimicrobial activities for drug development.

Acknowledgements

This work was supported in part by the Defense Threat Reduction Agency (DTRA) with contract HDTRA1-11-C-0011 (to M.E.J., J.L.C. and L.W.-M.F.), the UIC IAS Award for Faculty in the Natural Science (to L.W.-M.F.) and the UIC Chancellor's Graduate Research Fellowship (to N.M.W.). The authors thank Shahila Mehboob of UIC for the BaPurE gene, Loredana Huma for preparing CAIR and NAIR, and S. Tranchimand and T. Joseph Kappock of Purdue University for initial BaPurE enzyme activity assay. We also thank the RRC staff in the DNA Facility for the assistance with the RT-PCR instrument and the High-Throughput Screening Facility. The mass spectrometry facility at RRC was established in part by a grant from the Searle Funds at the Chicago Community Trust to the Chicago Biomedical Consortium.

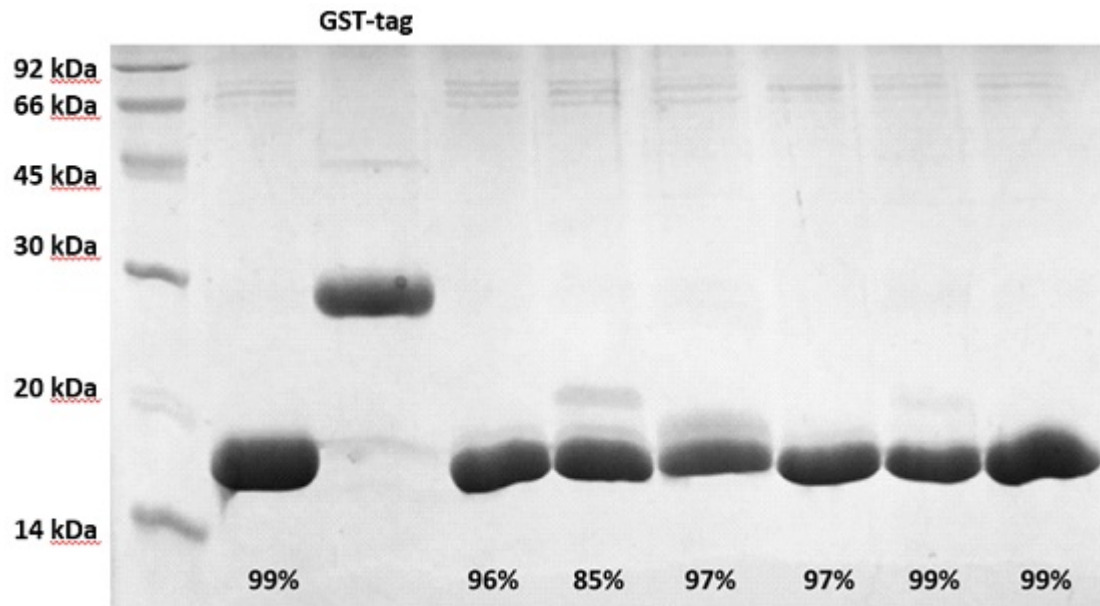
References and notes

- Tranchimand, S.; Starks, C. M.; Mathews, I. I.; Hockings, S. C.; Kappock, J. T. *Biochemistry* **2011**, *50*, 4623.
- Zhang, Y.; Morar, M.; Ealick, S. E. *Cell. Mol. Life Sci.* **2008**, *65*, 3699.
- Li, S.-X.; Tong, Y.-P.; Xie, X.-C.; Wang, Q.-H.; Zhou, H.-N.; Han, Y.; Zhang, Z.-Y.; Gao, W.; Li, S.-G.; Zhang, X. C.; Bi, R.-C. *J. Mol. Biol.* **2007**, *366*, 1603.

4. Firestine, S. M.; Wu, W.; Youn, H.; Davisson, V. J. *Bioorg. Med. Chem.* **2009**, *17*, 794.
5. Samant, S.; Lee, H.; Ghassemi, M.; Chen, J.; Cook, J. L.; Mankin, A. S.; Neyfakh, A. A. *PLoS Pathogen* **2008**, *4*, e37.
6. Lo, M.-C.; Aulabaugh, A.; Jin, G.; Cowling, R.; Bard, J.; Malamas, M.; Ellestad, G. *Anal. Biochem.* **2004**, *332*, 153.
7. Kranz, J. K.; Schalk-Hihi, C. *Methods Enzymol.* **2011**, *493*, 277.
8. Pantoliano, M. W.; Petrella, E. C.; Kwasnoski, J. D.; Lobanov, V. S.; Myslik, J.; Graf, E.; Carver, T.; Asel, E.; Springer, B. A.; Lane, P.; Salemme, F. R. *J. Biomol. Screening* **2001**, *6*, 429.
9. Koronakis, V. *FEBS Lett.* **2003**, *555*, 66.
10. Tuntland, M. L.; Johnson, M. E.; Fung, L. W.-M.; Santarsiero, B. D. *Acta Crystallogr., Sect. D* **2011**, *D67*, 870.
11. Tuntland, M. L.; Santarsiero, B. D.; Johnson, M. E.; Fung, L. W.-M. *Acta Crystallogr., Sect. D* **2014**, *D70*, 3057.
12. Wolf, N. M.; Abad-Zapatero, C.; Johnson, M. E.; Fung, L. W.-M. *Acta Crystallogr., Sect. D* **2014**, *D70*, 841. Corrigendum: **2014**, *D70*, 3087.
13. Louis-Jeune, C.; Andrade-Navarro, M. A.; Perez-Iraxeta, C. *Proteins: Struct., Funct., Bioinf.* **2012**, *80*, 374.
14. Boyle, M. P.; Kalliomaa, A. K.; Levnikov, V.; Blagova, E.; Fogg, M. J.; Brannigan, J. A.; Wilson, K. S.; Wilkinson, A. J. *Proteins: Struct., Funct., Bioinf.* **2005**, *61*, 674.
15. Laskowski, R. A. *Nucleic Acids Res.* **2009**, *37*, D355.
16. Sullivan, K. L.; Huma, L. C.; Mullins, E. A.; Johnson, M. E.; Kappock, T. J. *Anal. Biochem.* **2014**, *452*, 43.
17. Hoskins, A. A.; Morar, M.; Kappock, T. J.; Mathews, I. I.; Zaugg, J. B.; Barder, T. E.; Peng, P.; Okamoto, A.; Ealick, S. E.; Stubbe, J. *Biochemistry* **2007**, *46*, 2842.
18. Constantine, C. Z.; Starks, C. M.; Mill, C. P.; Ransome, A. E.; Karpowicz, S. J.; Francois, J. A.; Goodman, R. A.; Kappock, T. J. *Biochemistry* **2006**, *45*, 8193.
19. Meyer, E.; Leonard, N. J.; Bhat, B.; Stubbe, J.; Smith, J. M. *Biochemistry* **1992**, *31*, 5022.
20. Rasmussen, D. H.; MacKenzie, A. P. *Nature* **1968**, *220*, 1315.
21. Firestine, S. M.; Davisson, V. J. *J. Med. Chem.* **1993**, *36*, 3484.
22. Lee, H.; Zhu, T.; Patel, K.; Zhang, Y.-Y.; Truong, L.; Hevener, K. E.; Gatuz, J. L.; Subramanya, G.; Jeong, H.-Y.; Uprichard, S. L.; Johnson, M. E. *PLoS ONE* **2013**, *8*, e75144.
23. Ferguson, A. D.; Sheth, P. R.; Basso, A. D.; Paliwal, S.; Gray, K.; Fischmann, T. O.; Le, H. V. *FEBS Lett.* **2011**, *585*, 104.
24. Sainsbury, S.; Bird, L.; Rao, V.; Shepherd, S. M.; Stuart, D. I.; Hunter, W. N.; Owens, R. J.; Ren, J. J. *Mol. Biol.* **2011**, *405*, 173.
25. Sun, F.; Zhou, L.; Zhao, B. C.; Deng, X.; Cho, H.; Yi, C.; Jian, X.; Song, C. X.; Luan, C. H.; Bae, T.; Li, Z.; He, C. *Chem. Biol.* **2011**, *18*, 1032.
26. Zhang, J.-H.; Chung, T. D. Y.; Oldenburg, K. R. *J. Biomol. Screening* **1999**, *4*, 67.
27. Kozikowski, B. A.; Burt, T. M.; Tirey, D. A.; Williams, L. E.; Kuzmak, B. R.; Stanton, D. T.; Morand, K. L.; Nelson, S. L. *J. Biomol. Screening* **2003**, *8*, 205.
28. Cheng, X.; Hochlowski, J.; Tang, H.; Hepp, D.; Beckner, C.; Kantor, S.; Schmitt, R. *J. Biomol. Screening* **2003**, *8*, 292.
29. Popa-Burke, I. G.; Issakova, O.; Arroway, J. D.; Bernasconi, P.; Chen, M.; Coudurier, L.; Galasinski, S.; Jadhav, A. P.; Janzen, W. P.; Lagasca, D.; Liu, D.; Lewis, R. S.; Mohny, R. P.; Sepetov, N.; Sparkman, D. A.; Hodge, C. N. *Anal. Chem.* **2004**, *76*, 7278.
30. Hevener, K. E.; Mehboob, S.; Su, P.-C.; Truong, K.; Boci, T.; Deng, J.; Ghassemi, M.; Cook, J. L.; Johnson, M. E. *J. Med. Chem.* **2012**, *55*, 268.
31. Louie, A.; Heine, H. S.; Kim, K.; Brown, D. L.; VanScoy, B.; Liu, W.; Kinzig-Schippers, M.; Sorgel, F.; Drusano, G. L. *Antimicrob. Agents Chemother.* **2008**, *52*, 2486.
32. Firestine, S. M.; Poon, S.-W.; Mueller, E. J.; Stubbe, J.; Davisson, V. J. *Biochemistry* **1994**, *33*, 11927.
33. Richter, S. G.; Elli, D.; Kim, H. K.; Hendrickx, A. P. A.; Sorg, J. A.; Schneewind, O.; Missiakasa, D. *Proc. Nat. Acad. Sci. U.S.A.* **2013**, *110*, 3531.
34. Reynolds, R. C.; Ananthan, S.; Faaleolea, E.; Hobrath, J. V.; Kwong, C. D.; Maddox, C.; Rasmussen, L.; Sosa, M. I.; Thammavimol, E.; White, E. L.; Zhang, W.; Secrist, J. A., III. *Tuberculosis* **2012**, *92*, 72.
35. Hou, Z.; Nakanishi, I.; Kinoshita, T.; Takei, Y.; Yasue, M.; Misu, R.; Suzuki, Y.; Nakamura, S.; Kure, T.; Ohno, H.; Murata, K.; Kitaura, K.; Hirasawa, A.; Tsujimoto, G.; Oishi, S.; Fujii, N. *J. Med. Chem.* **2012**, *55*, 2899.
36. Cheng, T. J. R.; Wu, Y.-T.; Yang, S.-T.; Lo, K.-H.; Chen, S.-K.; Chen, Y.-H.; Huang, W.-I.; Yuan, C.-H.; Guo, C.-W.; Huang, L.-Y.; Chen, K.-T.; Shih, H.-W.; Cheng, Y.-S. E.; Cheng, W.-C.; Wong, C.-H. *Bioorg. Med. Chem.* **2010**, *18*, 8512.
37. Ates, O.; Kocabalkanli, A.; Cesur, N.; Otuk, G. *Il Farmaco* **1998**, *53*, 541.
38. de Oliveira, C. S.; Lira, B. F.; Barbosa-Filho, J. M.; Lorenzo, J. G. F.; de Athayde-Filho, P. F. *Molecules* **2012**, *17*, 10192.
39. Ramadoss, N. S.; Alumasa, J. N.; Cheng, L.; Wang, Y.; Li, S.; Chambers, B. S.; Chang, H.; Chatterjee, A. K.; Brinker, A.; Engels, I. H.; Keiler, K. C. *Proc. Nat. Acad. Sci. U.S.A.* **2013**, *110*, 10282.
40. Kreizinger, Z.; Makrai, L.; Helyes, G.; Magyar, T.; Erdelyi, K.; Gyuranecz, M. *J. Antimicrob. Chemother.* **2013**, *68*, 370.
41. Jones, M. E.; Visser, M. R.; Klootwijk, M.; Heisig, P.; Verhoef, J.; Schmitz, F.-J. *Antimicrob. Agents Chemother.* **1999**, *43*, 421.

APPENDIX B

Purity of recombinant *BaPurE*



APPENDIX C

Mass of recombinant *BaPurE*

Mass Spectrometry

Expected Mass = 17322.94 Daltons

Experimental Mass = 17322.1 Daltons

Difference = 0.84 Daltons



Order Number: 120160047

Sample: baPurE

Cilent and Sample Information

Name: Anna Kim

E-mail: akim94@uic.edu

Date: 03/18/2016

Method

The samples are first diluted with MS grade 0.1% FA in water at 1:1000 volume ratio. 1 μ L of diluted sample was injected into Thermo Orbitrap Velos Pro MS coupled to Agilent 1200 nano HPLC system.

Intact proteins were separated on a nanobore analytical column (75 μ m ID \times 10 cm) with an integral fritted nanospray emitter (PicoFrit[®], New Objective, Inc., Woburn, MA) using an Agilent Nano LC system, which was operated at a flow rate of 250 nL/min. A linear gradient of each 20 min 5–50% buffer B and 50–80% buffer B (80% ACN in 0.1% formic acid) was applied. This setup was extended with a trap column (150 μ m ID \times 1 cm) containing identical chromatographic material. MS data were acquired by a survey scan (ESI spray voltage 1.8kV, temperature 275 degrees, resolution 30,000 at m/z 400, m/z range 300-1800).

Results

There is one dominant species observed by MS, with a charge state distribution from charge 13 to 25.

The centroid Mw of species 1 is:

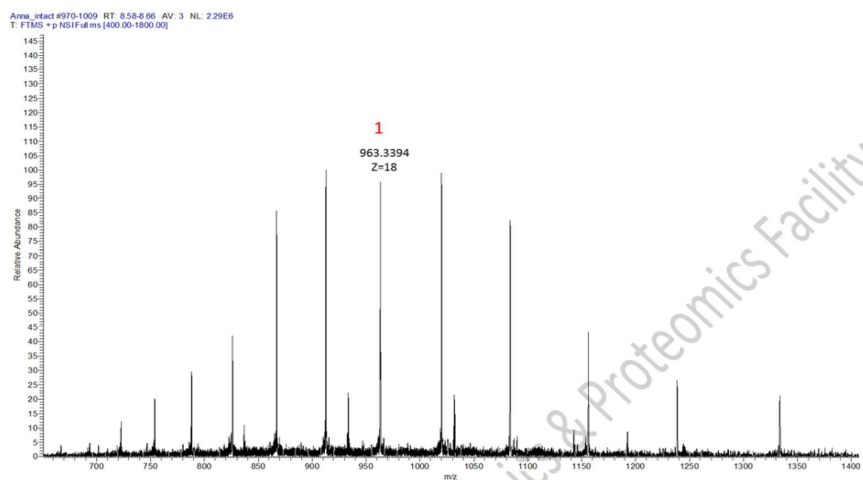
$$963.3394 \times 18 - 18 = 17322.1 \text{ Da}$$

According to the Mw provided by the client, species 1 is expected to be the target protein.



Order Number: 120160047

Sample: baPurE



Mass spectrometry, Metabolomics & Proteomics Facility

THE END